bioRxiv preprint doi: https://doi.org/10.1101/2024.04.16.589454; this version posted April 18, 2024. The copyright holder for this preprint (which was not certified by peer review) is the author/funder, who has granted bioRxiv a license to display the preprint in perpetuity. It is made available under aCC-BY-NC-ND 4.0 International license.

A generalized framework to identify SARS-CoV-2 broadly neutralizing antibodies

Fanchong Jian[1,2,3,#], Anna Z. Wec[4,#], Leilei Feng[5,6,#], Yuanling Yu[2], Lei Wang[5,6], Peng Wang[2], Lingling Yu[2], Jing Wang[1,2,7], Jacob Hou[4], Daniela Montes Berrueta[4], Diana Lee[4], Tessa Speidel[4], LingZhi Ma[4], Thu Kim[4], Ayijiang Yisimayi[1,2,7], Weiliang Song[1,2,7], Jing Wang[2], Lu Liu[2], Sijie
5 Yang[1,8], Xiao Niu[1,3], Tianhe Xiao[1,9], Ran An[2], Yao Wang[2], Fei Shao[2], Youchun Wang[2,10], Carole Henry[4], Simone Pecetta[4], Xiangxi Wang[5,6,*], Laura M. Walker[4,*], Yunlong Cao[1,2,8*]

[1]Biomedical Pioneering Innovation Center (BIOPIC), Peking University, Beijing 100871, China.
[2]Changping Laboratory, Beijing 102206, China.
10 [3]College of Chemistry and Molecular Engineering, Peking University, Beijing 100871, China.
[4]Moderna Inc., Cambridge, MA 02142, USA.
[5]CAS Key Laboratory of Infection and Immunity, National Laboratory of Macromolecules, Institute of Biophysics, Chinese Academy of Sciences, Beijing 100101, China.
[6]University of Chinese Academy of Sciences, Beijing 100049, China.
15 [7]School of Life Sciences, Peking University, Beijing 100871, China.
[8]Peking-Tsinghua Center for Life Sciences, Tsinghua University 100084, Beijing, China.
[9]Joint Graduate Program of Peking-Tsinghua-NIBS, Academy for Advanced Interdisciplinary Studies, Peking University 100871, Beijing, China.
[10]Institute of Medical Biology, Chinese Academy of Medical Science & Peking Union Medical
20 College, Kunming 650031, China.

[*]Correspondence: Xiangxi Wang (xiangxi@ibp.ac.cn), Laura M. Walker (laura.walker@modernatx.com), Yunlong Cao (yunlongcao@pku.edu.cn).

[#]These authors contributed equally.

25

bioRxiv preprint doi: https://doi.org/10.1101/2024.04.16.589454; this version posted April 18, 2024. The copyright holder for this preprint (which was not certified by peer review) is the author/funder, who has granted bioRxiv a license to display the preprint in perpetuity. It is made available under aCC-BY-NC-ND 4.0 International license.

Abstract

Monoclonal antibodies (mAbs) targeting the SARS-CoV-2 receptor-binding domain (RBD) showed high efficacy in the prevention and treatment of COVID-19. However, the rapid evolution of SARS-CoV-2 has rendered all clinically authorized mAbs ineffective and continues to stymie the development of next-generation mAbs. Consequently, the ability to identify broadly neutralizing antibodies (bnAbs) that neutralize both current and future variants is critical for successful antibody therapeutic development, especially for newly emerged viruses when no knowledge about immune evasive variants is available. Here, we have developed a strategy to specifically select for potent bnAbs with activity against both existing and prospective SARS-CoV-2 variants based on accurate viral evolution prediction informed by deep mutational scanning (DMS). By adopting this methodology, we increased the probability of identifying XBB.1.5-effective SARS-CoV-2 bnAbs from ~1% to 40% if we were at the early stage of the pandemic, as revealed by a retrospective analysis of >1,000 SARS-CoV-2 wildtype (WT)-elicited mAbs. From this collection, we identified a bnAb, designated BD55-1205, that exhibited exceptional activity against historical, contemporary, and predicted future variants. Structural analyses revealed extensive polar interactions between BD55-1205 and XBB.1.5 receptor-binding motif (RBM), especially with backbone atoms, explaining its unusually broad reactivity. Importantly, mRNA-based delivery of BD55-1205 IgG to human FcRn-expressing transgenic mice resulted in high serum neutralizing titers against selected XBB and BA.2.86 subvariants. Together, the ability to identify bnAbs via accurate viral evolution prediction, coupled with the speed and flexibility of mRNA delivery technology, provides a generalized framework for the rapid development of next-generation antibody-based countermeasures against SARS-CoV-2 and potentially other highly variable pathogens with pandemic potential.

bioRxiv preprint doi: https://doi.org/10.1101/2024.04.16.589454; this version posted April 18, 2024. The copyright holder for this preprint (which was not certified by peer review) is the author/funder, who has granted bioRxiv a license to display the preprint in perpetuity. It is made available under aCC-BY-NC-ND 4.0 International license.

Main

Severe acute respiratory syndrome coronavirus 2 (SARS-CoV-2) continues to rapidly evolve to evade antibody-mediated immunity induced by natural infection and vaccination, resulting in the emergence and circulation of highly evasive variant lineages like XBB.1.5 and JN.1 [1-4]. These
55 evasive variants are still continuously accumulating mutations in key antigenic sites in the RBD, such as L455, F456, and A475, which may significantly alter their antigenicity and further escape neutralizing antibodies elicited by repeated vaccination and infection [3,5-11].

Monoclonal neutralizing antibodies targeting the SARS-CoV-2 RBD have shown a high degree of efficacy in the treatment and prevention of COVID-19, especially in high-risk individuals who do
60 not mount robust immune responses to vaccination [12-17]. However, all previously approved anti-SARS-CoV-2 mAbs and mAb cocktail therapeutics, which were discovered before the emergence of variants of concern (VOCs), have lost clinical effectiveness against contemporary SARS-CoV-2 variants [18-21]. Since the emergence and rapid evolution of Omicron in 2021, numerous antibodies have been reported to be "broadly neutralizing" or "variant proof" based on their ability to neutralize
65 historical and existing SARS-CoV-2 variants, targeting either RBD, N-terminal domain (NTD), or subdomain 1 (SD1) of the virus Spike glycoprotein [22-29]. Unfortunately, the vast majority of these antibodies rapidly lost activity against newly emerged variants, raising questions about the criteria used to designate antibodies as broadly neutralizing and undermining confidence in the development of next-generation antibodies against SARS-CoV-2 [19,30,31]. Therefore, the development of a practical
70 strategy to identify bnAbs with neutralizing activity against both existing and prospective variants would greatly enhance the feasibility of developing future antibody-based countermeasures against SARS-CoV-2 that can outpace viral evolution and would have been invaluable at the early stages of a pandemic.

Previously, we employed high-throughput deep mutational scanning (DMS) on extensive panels of
75 mAbs to characterize the evolutionary pressures acting on the SARS-CoV-2 RBD to predict future mutation hotspots [30,32]. Building upon these efforts, we hypothesized that it would be possible to use pseudoviruses carrying predicted escape mutations to screen for mAbs that remain effective against prospective variants. These types of mAbs represent promising bnAb candidates for therapeutic

bioRxiv preprint doi: https://doi.org/10.1101/2024.04.16.589454; this version posted April 18, 2024. The copyright holder for this preprint (which was not certified by peer review) is the author/funder, who has granted bioRxiv a license to display the preprint in perpetuity. It is made available under aCC-BY-NC-ND 4.0 International license.

interventions against SARS-CoV-2. Here, we demonstrate that DMS-based mutation prediction can
80 significantly enhance the probability of identifying bnAbs that potently neutralize both existing and future variants. Using this framework, we identified a human IGHV3-66-derived Class 1 bnAb elicited by SARS-CoV-2 ancestral strain infection, designated as BD55-1205, which demonstrates extraordinary neutralization breadth against all existing variants as well as prospective variants with mutations within its targeting epitope. Delivery of mRNA-encoded BD55-1205 IgG in mice resulted
85 in high serum neutralizing titers against XBB.1.5, HK.3.1 and JN.1, providing evidence that mRNA technology could be leveraged for rapid deployment of anti-SARS-CoV-2 bnAbs. The ability to identify rare SARS-CoV-2 bnAbs via rational variant prediction, combined with the speed and flexibility of mRNA delivery technology, may enable the rapid development of next-generation antibody-based countermeasures against SARS-CoV-2, and potentially future pandemic pathogens.

90

Results

Retrospective assessment of SARS-CoV-2 NAbs

To date, anti-SARS-CoV-2 nAbs with potent neutralizing activity against currently circulating variants have been selected for clinical development. However, such NAbs have been repeatedly
95 escaped by Omicron and its subvariants, suggesting that activity against current variants does not translate into breadth against future variants[18,21,30]. To investigate the relationship between neutralization potency and breadth against SARS-CoV-2 variants, we studied a panel of 7,018 mAbs isolated from 7 previously described cohorts, which include individuals who were infected or vaccinated by ancestral SARS-CoV-2 (hereafter denoted as “WT”), individuals who experienced
100 SARS-CoV-1 infection in 2003/2004 and received 3-dose CoronaVac in 2021 (denoted as “SARS+WT”), convalescents who experienced BA.1, BA.2, or BA.5/BF.7 breakthrough infection (BTI) after 3-dose CoronaVac (denoted as BA.1 BTI, BA.2 BTI, BA.5/BF.7 BTI, respectively), and convalescents who experienced BA.1 or BA.2 BTI and were reinfected by BA.5/BF.7 (denoted as BA.1 or BA.2 BTI+BA.5/BF.7) [18,19,30,32,33]. Out of the 7,018 mAbs, we identified 1,637 potent
105 autologous NAbs, defined as IC_{50} < 0.05 μg/mL against the corresponding last-exposure variant (Fig. 1a).

bioRxiv preprint doi: https://doi.org/10.1101/2024.04.16.589454; this version posted April 18, 2024. The copyright holder for this preprint (which was not certified by peer review) is the author/funder, who has granted bioRxiv a license to display the preprint in perpetuity. It is made available under aCC-BY-NC-ND 4.0 International license.

To systematically investigate the breadth of NAbs isolated from various cohorts, we tested the neutralization activities of the 1,637 potent autologous NAbs against eight major SARS-CoV-2 variants, including B.1 (D614G), Omicron BA.1, BA.2, BA.5, BQ.1.1, XBB.1.5, HK.3, and JN.1
110 (Fig. 1b-d). Overall, only a minority of the potent autologous NAbs retained activity against subsequent Omicron variants. Among the 1,637 potent NAbs from 6 cohorts, only 296 and 147 mAbs demonstrated potent neutralization against XBB.1.5 and JN.1, respectively (Fig. 1b and Extended Data Fig. 1). Although there was an association between autologous and XBB.1.5 neutralization activity, NAbs with the strongest autologous neutralization activities generally lost
115 neutralization breadth against "future" variants (at that time); this phenomenon was particularly striking for NAbs obtained at the early stages of the pandemic from individuals infected or vaccinated with the ancestral strain (Fig. 1b). Among the 141 WT-elicited potent NAbs, only two (1%) remained potent against XBB.1.5, and only a single NAb potently neutralized all tested variants, including JN.1 (Fig. 1c). BA.1 and BA.2-elicited antibodies exhibited slightly better
120 tolerance to subsequent Omicron subvariants, but nevertheless, only 10/424 (2%) and 17/268 (7%) of the potent autologous NAbs showed activity against XBB.1.5, respectively (Fig. 1d). Although a higher proportion of mAbs from the BA.5/BF.7 BTI or reinfection cohorts neutralized BQ.1.1 and XBB.1.5, only 7% and 27% of these nAbs potently neutralized JN.1, respectively (Fig. 1d). Notably, the vast majority (85%) of SARS-CoV-1/SARS-CoV-2 D614G cross-reactive mAbs isolated from
125 the SARS+WT cohort showed abrogated activity against Omicron variants (Fig. 1c) [18,33]. Only five out of the 179 autologous potent NAbs from the SARS cohort potently neutralized all tested variants, and all of them belong to epitope group F3, targeting an epitope similar to that of SA55 [33]. We conclude that sarbecovirus-based identification of bnAbs does not guarantee neutralization breadth against emerging SARS-CoV-2 variants, and neutralization potency against circulating
130 variants at the time of isolation is not a sufficient metric to define neutralization breadth. Thus, a generalizable strategy to accurately identify bnAbs that retain activity against future SARS-CoV-2 variants is of paramount importance for the development of next-generation NAb-based therapies.

A generalized framework to select bnAbs

Previously, we demonstrated that the integration of DMS profiles accurately predicted mutations
135 that are likely to emerge during the evolution of viruses under humoral immune pressure [30,32]. We

bioRxiv preprint doi: https://doi.org/10.1101/2024.04.16.589454; this version posted April 18, 2024. The copyright holder for this preprint (which was not certified by peer review) is the author/funder, who has granted bioRxiv a license to display the preprint in perpetuity. It is made available under aCC-BY-NC-ND 4.0 International license.

hypothesized that it would be possible to efficiently identify bnAbs with retained activity against prospective variants by generating a panel of pseudovirus mutants encoding predicted future escape mutations and screening mAbs for activity against these viruses.

To validate this strategy, we retrospectively studied a collection of the mAbs elicited by SARS-CoV-
140 2 WT exposure, which would have been possible to obtain at the early stages of the pandemic [34-37]. First, we identified the RBD escape mutation hotspots of these mAbs by integrating their DMS escape profiles, which simulates the combined immune pressure of serum antibodies induced by primary SARS-CoV-2 exposure (Fig. 2a). This calculation also integrates codon preferences and the impact of each mutation on human ACE2 (hACE2) binding and RBD expression[30,32]. R346, K378,
145 K417, K444-G446, N450, L452, E484, F486, F490, and Q493 on RBD represented the major escape hotspots, and therefore we constructed mutants harboring mutations at these positions, named B.1+E484K and B.1-S1 to S5, to serve as the bnAb-screening pseudovirus panel (Fig. 2b). Specifically, the most prominent DMS mutation, E484K, was introduced into all of the designed mutants. We also selected the top-ranking amino acids from each of the other hotspots indicated by
150 DMS. The combinations of mutations in the constructed pseudovirus variants were designed to maintain hACE2 binding and avoid multiple mutations in the same epitope. As expected, these mutants, especially B.1-S3 (R346T + K417T + K444N + L452R + E484K + F486S), substantially escaped the majority of potent NAbs elicited by WT SARS-CoV-2 exposure (Fig. 2c and Extended Data Fig. 2a). Screening the NAb collection with the pseudovirus combination of B.1-S1 to S5
155 significantly enriches bnAbs capable of neutralizing all tested Omicron subvariants, and passing the filter of all five design mutants is shown to be an efficient indicator of broad neutralization against real-world Omicron variants (Fig. 2d-e).

Only 5 out of 141 NAbs remained potent (IC_{50} < 0.05 μg/mL) against all of the rationally designed evasive mutants (Fig. 2d). Notably, although the mutations of our predicted mutant sequences only
160 partially overlap with real-world Omicron variants, all 5 NAbs with activity against all rationally designed mutants effectively neutralized Omicron BA.1, BA.2, and BA.5. Importantly, the five selected bnAbs include the only two XBB.1.5-effective antibodies among the whole collection of 141 candidates, which corresponds to an increase in the probability of identifying "true" bnAbs from ~1% to 40%. Overall, our model correctly predicted the key escape mutations incorporated

bioRxiv preprint doi: https://doi.org/10.1101/2024.04.16.589454; this version posted April 18, 2024. The copyright holder for this preprint (which was not certified by peer review) is the author/funder, who has granted bioRxiv a license to display the preprint in perpetuity. It is made available under aCC-BY-NC-ND 4.0 International license.

165 during SARS-CoV-2 antigenic drift and allowed for the identification of a small subset of WT-elicited bnAbs with activity against future variants.

Additionally, we analyzed the whole panel of 320 NAbs from WT (n=141) and SARS+WT (n=179) cohorts, all of which could have been obtained early in the pandemic. Consistent with the results for WT-elicited NAbs, the neutralization activities of the SARS+WT-elicited NAbs against the designed
170 mutants predicted BA.5 and XBB.1.5 activity (Extended Data Fig. 2b-c).[38]. In contrast, most of the NAbs with the highest neutralization against B.1 (D614G) were escaped by XBB.1.5 and JN.1 (Fig. 2f and Extended Data Fig. 2d-e). Overall, 14 out of the 320 NAbs exhibited strong neutralization against the designed mutants, and 6 of them broadly neutralized JN.1 (Fig. 2g). The results validate our viral evolution prediction platform for the identification of rare, resilient bnAbs from a large
175 collection of antibodies isolated from convalescent or vaccinated individuals at the early stage of a pandemic.

BD55-1205 exhibits high barrier to escape

BD55-1205, a "Class 1" public antibody that utilizes the IGHV3-53/3-66 germline [34,39-41], was the only JN.1-effective bnAb identified from the WT-experienced donor group (Fig. 2g). Given BD55-
180 1205 exhibited broad neutralization against all major SARS-CoV-2 variants tested, we set out to determine whether it also demonstrated high barrier to escape under stringent in vitro conditions. We constructed XBB.1.5 S-pseudotyped replication-competent recombinant vesicular stomatitis virus (rVSV) and screened for escape mutations by serial passage of VSV in Vero cells over a range of concentrations (Fig. 3a and Extended Data Fig. 3a) [42-44]. For comparison, we also included the
185 previously described bNAb, SA55, and a non-competing pair of XBB.1.5-effective bnAbs (BD57-1520+BD57-2225, epitope group D4 and B, respectively) in this assay (Extended Data Fig. 3b-d). Surprisingly, BD55-1205 displayed similar resistance to viral escape as the cocktail of two antibodies, retaining neutralization until passage 6 (P6) (Fig. 3b and Extended Data Fig. 4d-e). In contrast, SA55, BD57-2225 and BD57-1520 were escaped after two or three passages (Fig. 3b and
190 Extended Data Fig. 4a-c). Substitutions L455P, Q493R/K, N417K, A435T, and D420Y were enriched in the BD55-1205-selected virus, which corresponds to critical residues interacting with Class 1 antibodies, as indicated by DMS selections with both BA.5 and XBB.1.5 RBD (Fig. 3c and

bioRxiv preprint doi: https://doi.org/10.1101/2024.04.16.589454; this version posted April 18, 2024. The copyright holder for this preprint (which was not certified by peer review) is the author/funder, who has granted bioRxiv a license to display the preprint in perpetuity. It is made available under aCC-BY-NC-ND 4.0 International license.

Extended Data Fig. 3c-d) [45]. To confirm the mutations selected by rVSV passage, we constructed mutant pseudoviruses predicted to escape BD55-1205, including XBB.1.5+L455P+Q493R,
195 XBB.1.5+N417K+A435T, XBB.1.5+D420Y+Q493K. In contrast to other antibodies we tested, we observed a reduction in the neutralizing potency of BD55-1205 but not complete loss of activity (Fig. 3d). Neutralization assays using soluble human ACE2 (hACE2) indicated lower receptor binding capability of the designed escape mutants compared to WT protein (Fig. 3d and Extended Data Fig. 5a-b), suggesting that the mutations abrogating BD55-1205 activity may result in reduced
200 viral fitness through disruption of receptor binding interactions.

We then evaluated BD55-1205 for neutralization against the latest real-world and prospective variants, including recently observed XBB, BA.2.86 or JN.1-derived subvariants with mutations on L455, F456, and A475, which are critical sites targeted by Class 1 mAbs. We determined the neutralization activities of BD55-1205 and a panel of NAbs targeting similar epitopes. BD55-1205
205 neutralization was largely retained against these variants, whereas other Class 1 NAbs lost significant activity against BA.2.86/JN.1 subvariants, including JN.1+F456L (identified as JN.1.11.1, a variant detected recently) (Fig. 3d). We subsequently assessed the binding affinity of BD55-1205 IgG to a panel of SARS-CoV-2 variant RBDs using surface plasmon resonance (SPR). Overall, BD55-1205 demonstrateed high apparent affinity to the tested RBD variants, ranging from
210 1 pM to 18 nM, partially explaining its exceptional tolerance to mutations within its epitope (Extended Data Fig. 5c-d).

To confirm the potent neutralization observed in the rVSV pseudotype assay system, we measured the neutralizing activity of BD55-1205 against authentic SARS-CoV-2 strains. Consistent with its broad neutralization against pseudoviruses, BD55-1205 potently inhibited live SARS-CoV-2 WT,
215 BA.5.2.1, FL.8, XBB.1.5.6, and JN.3 with IC_{50} values ranging from 0.007 to 0.026 ug/mL (Extended Data Fig. 6a). We also performed escape mutation selection with XBB.1.5.6 authentic virus under the selective pressure of BD55-1205, and found that even after 12 passages some assay wells still showed no sign of escape (Extended Data Fig. 6b). Amplicon sequencing of the viral genome revealed only one mutation within BD55-1205 epitope, S490Y (Extended Data Fig. 6c). Only 16
220 SARS-CoV-2 sequences with 490Y have been observed in the past 6 months, indicating its low real-world prevalence (between Sept 25 2023 and Mar 22 2024, data from CoV-Spectrum), and this

bioRxiv preprint doi: https://doi.org/10.1101/2024.04.16.589454; this version posted April 18, 2024. The copyright holder for this preprint (which was not certified by peer review) is the author/funder, who has granted bioRxiv a license to display the preprint in perpetuity. It is made available under aCC-BY-NC-ND 4.0 International license.

mutation is not a known escape hotspot of BD55-1205, or other Class 1 mAbs according to our DMS results. Instead, it is a known mutation that enhances ACE2 binding according to published DMS results [46].

225 **Structural analyses of BD55-1205**

To elucidate the structural mechanism underlying mAb BD55-1205's exceptional breadth, we determined the structure of XBB.1.5 S ectodomain trimer in complex with BD55-1205 Fab using Cryogenic electron microscopy (Cryo-EM) with single-particle reconstruction (Extended Data Fig. 7a). We asymmetrically reconstructed the complex structure at an overall resolution of 3.5 Å, with
230 one conformational state referred to as the three "open" RBDs observed (Extended Data Fig. 8a). To elucidate the antibody:RBD interface at a higher resolution we also determined the crystal structure of XBB 1.5 RBD alone in complex with BD55-1205 Fab (Extended Data Fig. 7b).

Consistent with its epitope defined by DMS, BD55-1205 is a Class 1 antibody that binds to the apical head of RBD, partially overlapping the receptor-binding motif (RBM) and the RBD core (Fig.
235 4a) [45]. In agreement with the defining features of other Class 1 antibodies derived from germlines IGHV3-53/3-66, BD55-1205 has a relatively short complementarity-determining region (CDR) H3 of 11 amino acids (using the IMGT convention) compared to the average length of human CDR H3 in unselected antibody repertoire [47,48]. The antibody footprint on RBD shows substantial overlap with the hACE2 receptor-binding sites (Fig. 4b and Extended Data Fig. 8b). The distal tip of the
240 RBM deeply inserts into a cavity formed by five CDRs, light chain (LC) CDRs 1 and 3 and heavy chain (HC) CDRs 1-3, resulting in a buried area of approximately 1,100 Å^2 (Extended Data Fig. 8c). Variable domains of the LC and HC contribute 30% and 70% of the buried surface area, respectively. The epitope of BD55-1205 encompasses over 20 residues, forming an extensive patch along the receptor binding ridge (Extended Data Fig. 8d). Binding of XBB.1.5 RBD by BD55-1205 is
245 primarily achieved through significant polar interactions, a sizeable proportion of which involve the RBD carbon backbone contacts. Seventeen hydrogen bonds are formed between the side chains of RBD residues R403, N405, T415, N417, D420, N487, Y489, Q493, Y501, H505 and HCDR residues Y33, S56, R97, R102, E104, as well as by LCDR residues N30, D93 (Fig. 4c). Additionally, 12 hydrogen bonds are formed between the backbone atoms of 9 RBD residues (L455, R457, K458,

bioRxiv preprint doi: https://doi.org/10.1101/2024.04.16.589454; this version posted April 18, 2024. The copyright holder for this preprint (which was not certified by peer review) is the author/funder, who has granted bioRxiv a license to display the preprint in perpetuity. It is made available under aCC-BY-NC-ND 4.0 International license.

250 Q474, A475, G476, S490, L492, G502) and HCDR sidechain (T28, R31, N32, Y33, P53, R102), as well as LCDR sidechain (S28) (Fig. 4d-g and Extended Data Fig. 9a). Furthermore, a network of hydrophobic interactions also contributes to the RBD:BD55-1205 interactions, involving G416, Y453, L455, F456 from XBB 1.5 RBD and Y33, Y52, F58, L99, I101 from the HC, as well as W94, P95 from the LC (Fig. 4h). For reference, we compared the binding interactions of BD55-1205 with 255 other published Class 1 (epitope group A1) NAbs that exhibit some extent of neutralization breadth, including P5S-1H1, P5S-2B10, BD-604 and Omi-42 (Fig. 4i-j and Extended Data Fig. 9a-c) [37,39,49]. Omi-42 is susceptible to A475V and L455F+F456L (FLip) mutations recently emergent in circulating XBB.1.5 and BA.2.86 lineages (Fig. 4i) [8]. The recognition of P5S-2B10 and P5S-1H1 is affected by N460K, which abrogates the hydrogen bonds on their interfaces (Fig. 4j). However, 260 because BD55-1205 makes more extensive interactions with the RBD backbone, it is not affected by these mutations, thus explaining its broad and resilient reactivity (Extended Data Fig. 9a). Despite the unaffected neutralization activity, L455S and A475V moderately dampen the affinity of BD55-1205 to RBD (Extended Data Fig. 5c). This could be explained by the potential impacts on the hydrophobic interactions involving L455 and a hydrogen bond between heavy chain N32 and 265 A475 backbone oxygen atom (Fig. 4h-i). Compared to the three IGHV3-53/3-66-derived NAbs (P5S-2B10, P5S-1H1, and BD-604), BD55-1205 has three unique residues in its heavy chain CDRs that were introduced by somatic hypermutation (SHM) or VDJ recombination and make contacts with the RBD backbone atoms: R31 on HCDR1, P53 on HCDR2, and R102 on HCDR3 (Extended Data Fig. 9b). These mutations, especially R31 and R102, introduce additional polar interactions on 270 the interface between BD55-1205 HC and RBD (Fig. 4k). We tested if contacts mediated by those residues could help explain broad neutralization capability by creating mutants of BD55-1205 carrying the R31S, P53S, or R102Y substitutions and also an IGHV germline-reverted version (BD55-1205-GLHV); the CDRH3 was left intact in mature form. Interestingly, all four mutant antibodies continued to neutralize BA.5, HK.3.1, JN.1 and JN.1+F456L pseudovirus with similar 275 potency to the parental antibody. However, BD55-1205-GLHV lost neutralizing activity against JN.1+F456L+A475V (Extended Data Fig. 9d). The apparent binding affinity of BD55-1205-GLHV to WT, BA.5, XBB.1.5, HK.3 and JN.1 RBD showed a substantial decrease of up to 52-fold depending on the variant tested (Extended Data Fig. 9e). These findings reveal that these three SHM

bioRxiv preprint doi: https://doi.org/10.1101/2024.04.16.589454; this version posted April 18, 2024. The copyright holder for this preprint (which was not certified by peer review) is the author/funder, who has granted bioRxiv a license to display the preprint in perpetuity. It is made available under aCC-BY-NC-ND 4.0 International license.

mutations unique to BD55-1205 compared to the other three antibodies only partially explain its
280 superior breadth, indicating that the 11-aa long HCDR3 sequence is likely the major determinant of the antibody's broad reactivity. Nevertheless, these IGHV SHMs enhance its RBD-binding affinity and potentially increase its ability to withstand further antigenic variation.

Delivery of mRNA-encoded BD55-1205 IgG results in broad and potent serum neutralization

Recombinant monoclonal antibodies or antibody cocktails have been demonstrated to be clinically
285 active in the prevention of symptomatic COVID [12,14,50-55]. Alternative means for delivery of therapeutic antibodies to patients – to the current standard of recombinant mAb products - could prove advantageous towards more rapid and widespread deployment in a pandemic or epidemic context. To that end, we encoded BD55-1205 in mRNA and formulated it into lipid nanoparticles (LNPs) for *in vivo* delivery. We also introduced the "LA" modification (M428L/N434A) in the Fc
290 region to enhance human FcRn binding at acidic pH, thereby improving the antibody half-life [56]. Formulated LNPs were delivered by intravenous injection to Tg32-SCID transgenic female mice that are homozygous for human fragment crystallizable neonatal receptor (FcRn) [57]. To assess BD55-1205 IgG expression kinetics, we quantified human IgG concentration in mouse sera collected at indicated time intervals following mRNA LNP delivery via ELISA(Fig. 5a). We
295 previously reported on in vivo pharmacokinetics of the mRNA-encoded Chikungunya virus E2 glycoprotein specific antibody CHKV-24 (mRNA-1944) determined in a Phase 1 clinical trial [58,59]. CHKV-24, with a human half-life of 69 days, was employed here as an expression and half-life benchmark and showed expression kinetics highly similar to BD55-1205 in the Tg32-SCID mouse (Fig. 5b) [58]. At 48 hours, serum antibody levels peaked at 505 μg/mL and 491 μg/mL for BD55-
300 1205 and CHKV-24, respectively (Fig. 5c). Given serum neutralizing titers are an established correlate of protection against SARS-CoV-2 [53-56], we also evaluated the neutralizing activities of the mouse sera against XBB.1.5, HK.3.1, and JN.1 pseudoviruses. BD55-1205 achieved high geometric mean peak serum neutralizing titers of 4496 against XBB.1.5, 5138 against HK.3.1 and 4608 against JN.1 at 48 hours post administration, underscoring the antibody's breadth (Fig. 5d-e). As expected,
305 we observed a significant correlation between human serum IgG concentrations and neutralization titers against the three variants at all timepoints (Fig. 5f). Together, we demonstrate that high serum antibody titers can be achieved following mRNA delivery in a mouse model. The speed and

bioRxiv preprint doi: https://doi.org/10.1101/2024.04.16.589454; this version posted April 18, 2024. The copyright holder for this preprint (which was not certified by peer review) is the author/funder, who has granted bioRxiv a license to display the preprint in perpetuity. It is made available under aCC-BY-NC-ND 4.0 International license.

flexibility of mRNA-LNP delivery, coupled with our bnAb prediction methodology, could accelerate the development and deployment of next-generation antibody therapeutics against SARS-
310 CoV-2.

Discussion

In this study, we interrogated a large collection of RBD-targeting mAbs from individuals with various SARS-CoV-2 exposure histories to demonstrate the feasibility of accurate and rational
315 variant prediction enabled by high-throughput DMS. Using this platform, we identified an IGHV3-66-derived, Class 1 bnAb named BD55-1205, which was elicited in a human donor with WT exposure only, and potently neutralizes all major SARS-CoV-2 variants. Interestingly, BD55-1205 was originally discovered in early 2021; however, we did not recognize its striking breadth of neutralization until the prevalence of XBB lineage in 2023. This highlights the necessity for a rapid
320 and reliable strategy for identifying truly broad neutralizing Abs and underscores the impact our prediction framework could make early in a pandemic.

Previously, we proposed a rational antibody selection strategy focused on the identification of NAbs targeting epitopes that are immunorecessive in SARS-CoV-2 vaccinated or convalescent individuals, thereby minimizing the impact of the selection pressure exerted by herd immunity of public antibody
325 responses [33]. However, this strategy to identify antibodies targeting subdominant epitopes can be challenging, particularly following the emergence of a novel pathogen when rare antibody sources that enrich such mAbs (e.g. previous SARS convalescents for the emergence of SARS-CoV-2) may not be readily available. Here, we highlight that true bnAbs need not exclusively target "rare" epitopes but rather should contact residues that withstand mutations occurring at these anticipated
330 mutation hotspots.

Our demonstration of high peak serum concentrations and neutralizing titers achievable with mRNA delivery of BD55-1205 in mice paves the way for rapid, flexible, and high-efficiency passive immunization against SARS-CoV-2. This is particularly beneficial for high-risk individuals who do not mount robust immune responses to vaccination. Altogether, the accurate viral evolution
335 prediction and mRNA-mAb delivery platform described here provide a practical framework for the

bioRxiv preprint doi: https://doi.org/10.1101/2024.04.16.589454; this version posted April 18, 2024. The copyright holder for this preprint (which was not certified by peer review) is the author/funder, who has granted bioRxiv a license to display the preprint in perpetuity. It is made available under aCC-BY-NC-ND 4.0 International license.

rapid identification and deployment of bnAbs to combat future SARS-CoV-2 variants. We also envision that this platform could be adapted to respond to other known pathogens with high pandemic potential, such as influenza, or even novel viruses responsible for "Disease X" in the future.

340

Acknowledgments

This project is financially supported by the Ministry of Science and Technology of China (2023YFC3043200), and Changping Laboratory (2021A0201; 2021D0102), and National Natural Science Foundation of China (32222030).

345 We wish to acknowledge the team at VisMederi Srl and Giulia Piccini, Alessandro Manenti and Emanuele Montomoli for their contribution of authentic virus assays. We also thank the Medicines and Healthcare Product Regulatory Agency (MHRA, United Kingdom) and Prof. Piet Maes (Rega Institute Leuven, Belgium) for providing the authentic SARS-COV-2 viruses. Additionally, we thank the team at IGA Technology Services and Davide Scaglione for their contribution of authentic 350 virus amplicon sequencing and data analysis services. We also thank Kath Hardcastle and the Comparative Medicine team at Moderna for the planning and execution of the in vivo studies.

Author contributions

Y.C. designed and supervised the study. F.J., A.Z.W., L.M.W. and Y.C. wrote the manuscript with inputs from all authors. L.F., L.W. and X.W. solved and analyzed the Cryo-EM structures. Y.Y. and 355 Youchun W. constructed pseudoviruses. P.W. and F.J. performed the rVSV escape screening experiments and data analysis. J.H. performed the authentic virus escape assays and data analysis. L.Y. performed the SPR experiments. P.W., L.Y., T.X., Yao W. and F. S. performed the pseudovirus neutralization assays. W.S., X.N., R.A. and Y.W. isolated the mAbs. J.W. (Changping Laboratory), L.L, L.Y. and F.S. performed protein expression and purification experiments. J.W. (BIOPIC) and 360 F.J. analyzed the DMS data. S.Y., L.F., and F.J. performed sequence analysis and illustration. A.Z.W., S.P., and L.M.W. conceptualized and planned the mRNA delivery study. K.W., D.M.B., D.L., and T.S. performed the mouse serum neutralization assays and data analysis. C.H., L.M., and T.K.

bioRxiv preprint doi: https://doi.org/10.1101/2024.04.16.589454; this version posted April 18, 2024. The copyright holder for this preprint (which was not certified by peer review) is the author/funder, who has granted bioRxiv a license to display the preprint in perpetuity. It is made available under aCC-BY-NC-ND 4.0 International license.

performed and supervised the pharmacokinetic ELISA assays.

Declaration of interests

365 Y.C. is listed as an inventor of provisional patent applications of SARS-CoV-2 RBD-specific antibodies involved in the study, including BD55-1205. The patent of BD55-1205 is licensed to Moderna. Y.C. is a co-founder of Singlomics Biopharmaceuticals. A.Z.W., J.H., D.M.B., D.L., T.S., L.M., T.K., K.W., C.H., S.P., and L.M.W. are full-time employees and holders of equity in Moderna Therapeutics. Other authors declare no competing interests.

370 **Data availability**

Information of the monoclonal antibodies involved in this study is included in Table S1. Cryo-EM data for structures have been deposited in the Protein Data Bank (PDB) with accession 8XE9 and 8XEA, and in the Electron Microscopy Data Bank (EMDB) with accession EMD-38283 and EMD-38284.

375

Figure legends

Figure 1 | Neutralization activities of RBD-targeting mAbs against SARS-CoV-2 variants

a, Neutralization of the 7,018 mAbs from individuals with 7 different immune histories against the corresponding last-exposure variant (autologous neutralization activity). Numbers and proportions

380 of potent autologous NAbs (IC_{50} < 0.05 μg/mL) are annotated above each group of points. The black circles indicate the geometric mean values of each group. **b**, Relationship between the autologous neutralization activities and XBB.1.5-neutralizing activities of the isolated mAbs. **c-d**, Neutralization activities of potent autologous NAbs against variants. Numbers and proportions of potent NAbs against each variant (IC_{50} < 0.05 μg/mL) are annotated.

385 **Figure 2 | Designed mutants based on mutation prediction define bnAbs**

a, Average escape profiles from DMS of mAbs (weighted by neutralization activities of each mAb against SARS-CoV-2 WT and the impact of each RBD mutation on ACE2 binding and RBD expression). **b**, Mutations harbored by the designed SARS-CoV-2 B.1-based mutants and real-world

bioRxiv preprint doi: https://doi.org/10.1101/2024.04.16.589454; this version posted April 18, 2024. The copyright holder for this preprint (which was not certified by peer review) is the author/funder, who has granted bioRxiv a license to display the preprint in perpetuity. It is made available under aCC-BY-NC-ND 4.0 International license.

variants on the key sites indicated by DMS-based prediction. **c**, Neutralization capability of the
390 mAbs from early cohorts (SARS+WT and WT) against the designed mutants and real-world Omicron variants. "S1-S5" indicates the highest IC_{50} against the five designed mutants. **d**, Number of NAbs from WT vaccinees or convalescents that pass the filter of designed mutants. Ratio of BA.1, BA.2, and BA.5-potent NAbs among the passed NAbs are annotated above the bar of each combination of filters. **e**, Significance for the enrichment of BA.1, BA.2, BA.5, BQ.1.1, or XBB.1.5-
395 potent NAbs within NAbs that are from WT vaccinees or convalescents and pass each filter of designed mutants (hypergeometric test). **f**, Ratio of BA.5 or XBB.1.5-potent NAbs within the NAbs with "top k" neutralization activities against D614G or S1-S5. **g**, Charcteristics of NAbs isolated from early cohorts that pass the designed filters.

Figure 3 | BD55-1205 exhibits extraordinary resistance to viral escape

400 **a**, Schematic for the rVSV-based escape mutation screening assays. **b**, Results of the escape screening by rVSV passaging under the NAb pressure. Values in the P1-P10 columns of the table indicate the highest concentration of NAb that was escaped by rVSV in the first passage to the tenth passage. The mutations observed in the final passage of rVSV were determined by Sanger sequencing and are annotated in the last column. **c**, DMS escape profiles (based on XBB.1.5 RBD)
405 of the NAbs evaluated in the rVSV assays. The average profile of antibodies in epitope group A1 is also shown for comparison with BD55-1205. **d**, Neutralization of BD55-1205 and other NAbs against designed escape mutants according to rVSV screening and DMS profiles, and real-world emerging and prospective mutants with mutations in the BD55-1205 epitope.

Figure 4 | Structural basis for the broad reactivity of BD55-1205

410 **a**, Structural model of SARS-CoV-2 XBB.1.5 RBD in complex with BD55-1205 from Cryo-EM data. **b**, Overlay of BD55-1205 and hACE2 binding footprints on XBB.1.5 RBD. **c**, Polar interactions between BD55-1205 and XBB.1.5 RBD side chain atoms. **d**, RBD backbone interactions with BD55-1205 Fab. **e-g,** Polar interactions between BD55-1205 heavy chain or light chain and XBB.1.5 RBD backbone atoms in the binding interface. Yellow dashed lines indicate
415 potential polar interactions. RBD, heavy chain, and light chain are colored in blue, magenta, and cyan, respectively. **h**, Hydrophobic interaction between RBD and BD55-1205. **i-k**, Comparison of

bioRxiv preprint doi: https://doi.org/10.1101/2024.04.16.589454; this version posted April 18, 2024. The copyright holder for this preprint (which was not certified by peer review) is the author/funder, who has granted bioRxiv a license to display the preprint in perpetuity. It is made available under aCC-BY-NC-ND 4.0 International license.

the RBD interactions with BD55-1205 and other Class 1 NAbs (PDB: Omi-42, 7ZR7; P5S-1H1, 7XS8; P5S-2B10, 7XSC; BD-604, 8HWT).

Figure 5 | mRNA delivery of BD55-1205 in mice

420 **a**, A schematic of the experimental design for delivery of BD55-1205 and CHKV-24 via LNP encapsulated mRNA in Tg32-SCID mice. Female mice, 4 per group, received 0.5 mg/kg dose by intravenous injection on day 0 and serum was collected at the indicated time points. **b**, Serum concentration of BD55-1205 and a benchmark antibody CHKV-24 plotted over time. Geometric mean with error (95% confidence interval) is shown by outlined circles with error bars; solid 425 symbols indicate individual animals. A biexponential curve was fitted to the data. Two independent in vivo experiments were combined, each with n=4 animals per group. **c**, Peak serum concentration, occurring at 48 hours post LNP administration, for BD55-1205 and CHKV-24. Bar height and number above the bar indicate the geometric mean; error bars indicate 95% confidence intervals; empty symbols indicate individual animals. NS, not significant (Wilcoxon rank-sum test). **d**, Half-430 maximal inhibitory dilutions (ID_{50}) of the mouse sera against XBB.1.5, HK.3.1, and JN.1 VSV pseudoviruses for BD55-1205 plotted over time. Geometric mean values are shown as the colored empty circles and lines. The ID_{50} values for individual mouse serum samples are shown as colored points and lines. **e**, Peak serum neutralizing titers in mice receiving BD55-1205 mRNA against the three indicated viral variants. Bar height and number above the bar indicate the geometric mean; 435 error bars indicate the 95% confidence interval; empty symbols indicate individual animals**.** NS, not significant (Wilcoxon rank-sum test applied to any pair of variants). **f**, Scatter plots showing the correlation between serum hIgG concentrations and the ID_{50} against the three variants at indicated timepoints. Pearson correlation coefficients (R) and the corresponding significance p-values are annotated.

440

Extended Data Figures

Extended Data Fig. 1 | Neutralization distribution of mAbs collected

Distribution of the neutralization activities (IC_{50}) of potent autologous NAbs against XBB.1.5 and

bioRxiv preprint doi: https://doi.org/10.1101/2024.04.16.589454; this version posted April 18, 2024. The copyright holder for this preprint (which was not certified by peer review) is the author/funder, who has granted bioRxiv a license to display the preprint in perpetuity. It is made available under aCC-BY-NC-ND 4.0 International license.

JN.1.

445 **Extended Data Fig. 2 | Neutralization activities for the identification of bnAbs**

a, Heatmap of the neutralization activities (IC_{50}) for the mAbs from early cohorts (SARS+WT and WT) against the designed mutants and real-world Omicron variants. “S1-S5” indicates the highest IC_{50} against the five designed mutants. **b**, Significance for the enrichment of BA.1, BA.2, BA.5, BQ.1.1, or XBB.1.5-potent NAbs within NAbs that were from WT or SARS+WT cohort pass each
450 filter of designed mutants (hypergeometric test). **c**, Number of NAbs from WT or SARS+WT cohort that pass the filter of designed mutants. Ratio of BA.1, BA.2, and BA.5-potent NAbs among the passed NAbs are annotated above the bar of each combination of filter. **d-e**, Ratio of BA.5 or JN.1-potent NAbs within the NAbs from WT cohort (d), or WT in addition to SARS+WT cohort (e) with “top k” neutralization activities against D614G or S1-S5.

455 **Extended Data Fig. 3 | DMS and rVSV screening indicate the epitopes targeted by bnAbs**

a, Schematic for the construction of the SARS-CoV-2 XBB.1.5 Spike-pseudotyped rVSV genome. **b**, Information of the two non-competing NAbs utilized in the rVSV screening assays. **c**, DMS escape profiles (based on BA.5 RBD) of the NAbs involved in the rVSV assays. The average profile of antibodies in epitope group A1 is also shown for comparison with BD55-1205. **d**, Key RBD sites
460 that may be involved in the binding of NAbs (BD55-1205, SA55, BD57-1520 and BD57-2225) as determined by rVSV screening (green) and DMS (red) are marked on the structural model of XBB.1.5 RBD (PDB: 8WRL).

Extended Data Fig. 4 | Raw images of the rVSV escape mutants screening assays

Raw images of the rVSV passages under the pressure of SA55 (a), BD57-2225 (b), BD57-1520 (c),
465 BD57-2225+1520 (d), and BD55-1205 (e). Red rectangles indicate the well for the next passage, and blue rectangles indicate the well for Sanger sequencing.

Extended Data Fig. 5 | SARS-CoV-2 variant RBD-binding affinity of BD55-1205 and hACE2

a, Inhibition curves of soluble hACE2 against SARS-CoV-2 Omicron variant pseudoviruses. **b**, IC_{50} of soluble hACE2 against the variants. Geometric mean values are shown and annotated above the
470 bars, and the circles indicate each replicate. **c**, RBD apparent binding affinity of BD55-1205 IgG to

bioRxiv preprint doi: https://doi.org/10.1101/2024.04.16.589454; this version posted April 18, 2024. The copyright holder for this preprint (which was not certified by peer review) is the author/funder, who has granted bioRxiv a license to display the preprint in perpetuity. It is made available under aCC-BY-NC-ND 4.0 International license.

SARS-CoV-2 RBD variants determined by SPR assays. Geometric mean of apparent K_D (nM) is shown and annotated above the bars, and the circles indicate each replicate. **d,** SPR sensorgrams of the binding of BD55-1205 to six major SARS-CoV-2 RBD variants. The association and dissociation kinetic coefficients (k_a, k_d), and the apparent dissociation equilibrium constant (K_D) are
475 annotated.

Extended Data Fig. 6 | BD55-1205 inhibits SARS-CoV-2 authentic virus

a, IC_{50} of BD55-1205 against authentic SARS-CoV-2 isolates. Geometric mean IC_{50} (μg/mL) is labeled above the points and geometric SD is indicated by error bars. **b**, Number of wells in the plate that show protection from CPE in each passage in the escape screening assay using XBB.1.5.6
480 authentic virus. Asterisks indicate low-level/ambiguous CPE observation. **c**, Spike mutations observed in viral S protein resolved using amplicon-based deep sequencing of viral genome at each passage with BD55-1205 selection.

Extended Data Fig. 7 | Workflow for the processing of Cryo-EM data

a, Workflow for the processing of raw Cryo-EM images for XBB.1.5 Spike in complex of BD55-
485 1205. **b**, Workflow for the processing of raw Cryo-EM images for XBB.1.5 RBD in complex of BD55-1205.

Extended Data Fig. 8 | Structure of BD55-1205 in complex with Spike and RBD

a, Structure of BD55-1205 in complex of XBB.1.5 Spike with 3 RBD "up". **b**, The epitope targeted by BD55-1205 is highly similar to hACE2 receptor binding sites. **c**, BD55-1205 interacts with
490 XBB.1.5 RBD via heavy chain and light chain CDRs. **d**, RBD residues in SARS-CoV-2 variants targeted by BD55-1205. Conserved residues are marked in green, and the other residues targeted by BD55-1205 are marked in blue.

Extended Data Fig. 9 | Comparison of BD55-1205 and Class 1 NAbs

a, A list of all polar interactions between SARS-CoV-2 variant RBD and BD55-1205. Interactions
495 involving RBD backbone atoms are marked in red. **b**, Alignment of the heavy chains of BD55-1205, P5S-2B10, P5S-1H1, and BD-604. Heavy chain CDRs are marked in blue rectangles. Potential key mutations of BD55-1205 are marked in red rectangles. **c**, Footprints of the four antibodies on SARS-

bioRxiv preprint doi: https://doi.org/10.1101/2024.04.16.589454; this version posted April 18, 2024. The copyright holder for this preprint (which was not certified by peer review) is the author/funder, who has granted bioRxiv a license to display the preprint in perpetuity. It is made available under aCC-BY-NC-ND 4.0 International license.

CoV-2 RBD. **d**, Neutralization of BD55-1205 with mutations on the heavy chain. **e**, RBD-binding affinity of BD55-1205 with mutations on the heavy chain. Geometric mean values are shown as
500 bars, and the circles indicate each replicate.

Methods

Cell culture

For viral escape assay, VERO E6 cells were cultured as described previously [1]. Briefly, African
505 green monkey kidney VERO E6 cells (American Type Culture Collection [ATCC] #CRL-1586/VERO C1008) were maintained in Dulbecco's Modified Eagle's Medium (DMEM) high Glucose (Euroclone, Pero, Milan) supplemented with 2 mM L-Glutamine (Euroclone, Pero, Milan), 100 units/mL of penicillin - streptomycin (Gibco, Life Technologies) ("complete DMEM" medium) and 10% Fetal Bovine Serum (FBS) (Euroclone, Pero, Milan).
510 For plaque reduction neutralization test (PRNT), VERO E6 were maintained in MEM (Gibco, Life Technologies) supplemented with 2 mM L-Glutamine, 100 units/mL of penicillin - streptomycin, Non-Essential Amino Acids (Gibco, Life Technologies), HEPES 25mM (Gibco, Life Technologies) and 10% FBS ("PRNT MEM"). Cells were incubated at 37°C in a humidified atmosphere with 5% CO2 and passaged every 3 to 4 days.
515

Antibody expression and purification

Antibody heavy and light chain genes were codon-optimized and synthesized by GenScript, separately inserted into vector plasmids (pCMV3-CH, pCMV3-CL or pCMV3-CK) via infusion (Vazyme). The plasmids were co-transfected into Expi293F cells (Thermo Fisher) using
520 polyethylenimine transfection. The transfected cells were cultured at 36.5°C in 5% CO_2 and 175 rpm for 6-10 days. The expression fluid was collected and centrifuged, and then supernatants containing monoclonal antibodies were purified by Protein A magnetic beads (Genscript). The purified mAb samples were verified by SDS-PAGE.

525 ### Pseudovirus neutralization assays

bioRxiv preprint doi: https://doi.org/10.1101/2024.04.16.589454; this version posted April 18, 2024. The copyright holder for this preprint (which was not certified by peer review) is the author/funder, who has granted bioRxiv a license to display the preprint in perpetuity. It is made available under aCC-BY-NC-ND 4.0 International license.

SARS-CoV-2 wildtype Spike glycoprotein sequence is from the reference genome (MN908947). Spike-pseudotyped viruses of SARS-CoV-2 variants were prepared based on a vesicular stomatitis virus (VSV) pseudovirus packaging system as described previously [60]. Briefly, variants' spike plasmid is constructed into pcDNA3.1 vector (BA.1, A67V+HV69-
530 70del+T95I+G142D+V143del+Y144del+Y145del+N211del+L212I+ins214EPE+G339D+S371L+S373P+S375F+K417N+N440K+G446S+S477N+T478K+E484A+Q493R+G496S+Q498R+N501Y+Y505H+T547K+D614G+H655Y+N679K+P681H+N764K+D796Y+N856K+Q954H+N969K+L981F; BA.2, T19I+LPPA24-27S+G142D+V213G+G339D+S371F+S373P+S375F+T376A+D405N+R408S+K417N+N440K+
535 S477N+T478K+E484A+Q493R+Q498R+N501Y+Y505H+D614G+H655Y+N679K+P681H+N764K+D796Y+Q954H+N969K; BA.5, BA.2+HV69-70del+L452R+F486V+R493Q; BQ.1.1, BA.5+R346T+K444T+N460K; XBB.1.5, BA.2+V83A+Y144del+H146Q+Q183E+V213E+G339H+R346T+L368I+V445P+G446S+N460K+F486P+F490S+R493Q; HK.3, XBB.1.5+Q52H+L455F+F456L; JN.1,
540 BA.2+ins16MPLF+R21T+S50L+H69-+V70-+V127F+Y144-+F157S+R158G+N211-+L212I+L216F+H245N+A264D+I332V+D339H+K356T+R403K+V445H+G446S+N450D+L452W+L455S+N460K+N481K+V483-+A484K+F486P+R493Q+E554K+A570V+P621S+H681R+S939F+P1143L). G*ΔG-VSV (VSV-G pseudotyped virus, Kerafast) and SARS-CoV-2 spike plasmid were transfected to 293T cells (American Type Culture Collection [ATCC], CRL-
545 3216). After culture, the pseudovirus in the supernatant was harvested, filtered, aliquoted, and frozen at −80°C for further use.

Huh-7 cell line (Japanese Collection of Research Bioresources [JCRB], 0403) was used in pseudovirus neutralization assays. Purified mAbs were serially diluted in culture media and mixed with pseudovirus, and incubated for 1 h in a 37°C incubator with 5% CO_2. Then, the digested Huh-
550 7 cells were seeded in the antibody-virus mixture. After one day of culture in the incubator, the supernatant was discarded, and D-luciferin reagent (PerkinElmer, 6066769) was added into the plates. After 2 min incubation in darkness, cell lysis was transferred to detection plates. The luminescence values were detected and recorded with a microplate spectrophotometer (PerkinElmer, HH3400). IC_{50} was determined by fitting four-parameter logistic regression models.

bioRxiv preprint doi: https://doi.org/10.1101/2024.04.16.589454; this version posted April 18, 2024. The copyright holder for this preprint (which was not certified by peer review) is the author/funder, who has granted bioRxiv a license to display the preprint in perpetuity. It is made available under aCC-BY-NC-ND 4.0 International license.

555 **Authentic virus propagation and titration.**

Authentic SARS-CoV-2 Omicron variant XBB.1.5.6 was kindly provided by Rega Institute Leuven (Belgium). Live Omicron variant BA.2.86 sub-lineage JN.3 (catalogue number #101123) was kindly provided by the Medicines and Healthcare Product Regulatory Agency (MHRA, United Kingdom). Viral propagation of both strains was carried out as previously described [61]. Briefly, 175cm2 flasks

560 were inoculated with VERO E6 cells diluted in complete DMEM 2% FBS (1x106 cells/mL). Cells were incubated at 37°C, 5% CO2 in a humidified atmosphere for 20-24 hours, then the sub-confluent cell monolayer was washed twice with sterile Dulbecco's phosphate buffered saline (DPBS) and inoculated with the SARS-CoV-2 virus at a multiplicity of infection (MOI) of 0.001. After 1 hour at 37°C, 5% CO2, the flasks were filled with 50 mL of complete DMEM 2% FBS and kept at 37°C,

565 5% CO2. Flasks were inspected daily under an optical microscope to check for signs of cytopathic effect (CPE) in the VERO E6 monolayer. Once CPE was developed in at least 80-90% of the cell monolayer, the supernatants of the infected cell culture were collected, centrifuged at 1000 rpm for 5 minutes (4°C), aliquoted and stored at -80°C.

For viral escape assay, a titration of the propagated Omicron variant XBB.1.5.6 was performed in

570 96-well plates containing confluent VERO E6 cells, by means of the 50% tissue culture infectious dose assay (TCID50). Cells infected with serial 10-fold dilutions of the virus (from 10-1 to 10-11) were incubated at 37°C, 5% CO2 and monitored for signs of virus-induced CPE under an inverted optical microscope for 4 days. The end-point viral titer, defined as the reciprocal of the highest viral dilution resulting in at least 50% CPE in the inoculated wells, was calculated according to the Reed

575 and Muench formula [62]. Titration of plaque forming unit/ml (PFU/ml) of SARS-CoV-2 Omicron XBB.1.5.6 and JN.3 variants was performed in pre-seeded VERO E6 cells in 96-well plates. Briefly, cells were infected with serial 0.5 Log-fold dilutions of the virus (from 10-1 to 10-6) and incubated for 24 h at 37°C, 5% CO2. The viral titer was calculated by PFU counting.

580 **Authentic virus escape mutant escape assay**

For the Viral Escape Assay, a standard concentration of authentic XBB.1.5.6 virus was sequentially passaged in VERO E6 cells in the presence of serially diluted SARS-CoV-2-specific-monoclonal antibodies. The viral escape assay was performed as previously reported [61]. Briefly, 12 serial two-

bioRxiv preprint doi: https://doi.org/10.1101/2024.04.16.589454; this version posted April 18, 2024. The copyright holder for this preprint (which was not certified by peer review) is the author/funder, who has granted bioRxiv a license to display the preprint in perpetuity. It is made available under aCC-BY-NC-ND 4.0 International license.

fold dilutions of each antibody sample were prepared in DMEM 2% FBS (starting concentration of antibody before virus addition: 20 µg/mL). Each serially diluted sample was added to the wells of a 24-well plate, pre-seeded with VERO E6 cells (2x105 cells/well). Then, a virus solution containing 105 TCID50 of authentic SARS-CoV-2 Omicron variant XBB.1.5.6 was dispensed in each antibody-containing well, and in wells dedicated to virus-only control.

The plates were then incubated for 1 h at 37°C, 5% CO_2, to allow binding of the antibody sample to the virus. The virus-sample mixture was then transferred into the wells of a 24-well plate containing previously seeded VERO E6 cells, to allow their infection from the unbounded residual virus. The plates were incubated for 7 days at 37°C, 5% CO_2, then cells were examined for the presence of virus-induced cytopathic effect (CPE) using an inverted optical microscope. The content of the well corresponding to the highest antibody concentration showing complete CPE was collected and further diluted to be used as the viral solution in the next virus passage. The potency of each antibody was recorded at each virus passage and expressed as Inhibitory Concentration 100% (IC100) (i.e., the lowest antibody concentration inhibiting development of CPE). The virus pressured with SARS-CoV-2 antibody was passaged in cell cultures along with the antibody sample of interest until CPE was observed at higher antibody concentrations. At each passage, both the virus pressured with the antibody sample of interest and the virus-only control were harvested, propagated for one round of passaging in different 25cm2 flasks (pre-seeded with 1x105 VERO E6 cells/mL), aliquoted and stored at -80°C to be used for RNA extraction and sequencing. The sequences of both these types of samples can assist in distinguishing between adaptation to cell culture conditions and escape mutations. Parallel titrations of each antibody-pressured virus were performed at every passage in 96-well plates containing pre-seeded VERO E6 cells (1.5x104 cells/well), to monitor the viral titer at each test.

RNA Extraction

The RNA extraction to obtain the viral genetic material for next-generation sequencing was performed using biocomma® Nucleic Acid Purification Kit (Spin Column) commercial kit (MNP027-1E, Biocomma Limited), as described previously [61]. Briefly, 300 µL of viral sample were mixed with 500 µL of "Buffer GLX", vortexed for 1 minute and incubated at room temperature (RT) for at least 5 minutes to allow virus lysis. The supernatant was then transferred into a spin column

bioRxiv preprint doi: https://doi.org/10.1101/2024.04.16.589454; this version posted April 18, 2024. The copyright holder for this preprint (which was not certified by peer review) is the author/funder, who has granted bioRxiv a license to display the preprint in perpetuity. It is made available under aCC-BY-NC-ND 4.0 International license.

inserted in a collection tube and centrifuged at 12,000 rpm for 1 minute at RT. After discarding the flow-through, 500 µL of "Buffer PD" (previously re-suspended with isopropanol) were added,
615 centrifuged as before, followed by elimination of the eluted solution. The column was then washed with 700 µL of "Buffer PW" (previously re-suspended in absolute ethanol), centrifuged and eluted as before. This step was repeated twice. The spin column was then centrifuged at 12,000 rpm for 2 minutes and left with open lid for 5 minutes to allow evaporation of residual ethanol. The column was placed in a new collection tube and 60 µL of RNAse-free ddH20 were added. After a 2 minutes
620 incubation at RT, the column was centrifuged for 2 minutes at 12,000 rpm to elute and collect the RNA, which was stored at -80°C until shipment for sequencing.

Deep sequencing of authenic virus from escape assay and data analysis

The cDNA preparation was performed in a total volume of 40 uL by following manufacturer's
625 recommendations for SuperScript™ II Reverse Transcriptase (Life Technologies 18064022), Random Hexamers (50 µM) (Euroclone N8080127) and RNaseOUT™ Recombinant Ribonuclease Inhibitor (Life Technologies 10777019) suing a thermocycler. Sars-CoV-2 genome amplicons were generated using ARTIC v3.5.2 panel (IDT, cat # 10016495) , together with a set of custom oligo pools to improve coverage on the RBD domain sequence. The Celero™ DNA-Seq kit (NuGEN,
630 San Carlos, CA, USA) was then used for library preparation following the manufacturer's instructions. Both input and final libraries were quantified by Qubit 2.0 Fluorometer (Invitrogen, Carlsbad, CA, USA) and quality tested by Agilent 2100 Bioanalyzer High Sensitivity DNA assay (Agilent technologies, Santa Clara, CA, USA). Libraries were then prepared for sequencing and sequenced on Illumina NovaSeq6000 (Illumina, San Diego, CA, USA) in paired-end 150 mode to
635 generate a minimum of 5 million reads per sample.

Raw sequencing reads were first processed by removing PCR primer sequences using Cutadapt v2.6, with parameters set to discard untrimmed pairs and ensure a minimum read length of 50 bp. Quality trimming was performed with Fastp v0.20.0 to retain bases with a Phred score ≥ Q30. The resulting high-quality reads were aligned to the NCBI Reference Sequence accession "OQ063792.1".
640 Subsequent filtering wiat a custom script removed reads with low mapping quality or suboptimal alignment characteristics. Variants were identified using GATK HaplotypeCaller v4.1.6.0 and

bioRxiv preprint doi: https://doi.org/10.1101/2024.04.16.589454; this version posted April 18, 2024. The copyright holder for this preprint (which was not certified by peer review) is the author/funder, who has granted bioRxiv a license to display the preprint in perpetuity. It is made available under aCC-BY-NC-ND 4.0 International license.

normalized with Bcftools norm v1.9. A consensus sequence for each sample was generated by applying filtered variants to the reference sequence using Bcftools consensus, with low-coverage positions masked. Coverage was assessed with Bedtools genomecov v2.29.2.

645

Authentic virus plaque reduction neutralization

Determination of Half maximal inhibitory concentration (IC50) was performed in VERO E6 cells by immunodetection of viral antigen. Briefly, 100 PFU/well of SARS-CoV-2 Omicron XBB.1.5.6 or Omicron JN.3 were incubated 1h with 5% CO_2 with serial 4-fold dilutions of monoclonal

650 antibodies (range 50-0.003 nM). At the end of incubation, pre-seeded VERO E6 cells in 96-well plates were adsorbed with virus-sample mixture for 1 h at 37 °C with 5% CO_2. After removal of virus inoculum, the overlay media was added at each well and plates were incubated for 24 h at 37 °C with 5% CO_2.

The immunodetection assay was performed as described previously [63] with minor modifications.

655 Briefly, cells were fixed for 3 hours with formalin 10% (Sigma Aldrich), and permeabilized for 20 min with 0.1% Triton X-100 (Sigma Aldrich). After washing with PBS 1X (Thermofisher Scientific) containing 0.05% Tween 20 (Sigma Aldrich), plates were incubated for 1 h with monoclonal anti-nucleocapsid virus mouse antibody (Genscript) diluted 1:1000 in blocking buffer (PBS 1X containing 1% BSA (Sigma Aldrich) and 0.1% Tween 20). After washing, cells were incubated for

660 1 h with a polyclonal Horseradish Peroxidase (HRP)-coupled anti-mouse IgG secondary antibody (Thermofisher Scientific) diluted 1:2000 in blocking buffer. Next, cells were washed and the TrueBlue™ Peroxidase Substrate (Sera Care) was added to each well.

Detection of microplaques was performed with ImmunoSpot® S6 Ultra-V Analyzer (C.T.L.) reader using BioSpot® software according to instrument specifications. The IC50 for each sample was

665 calculated with GraphPad Prism® Software using the dose-response inhibition category and apply log(inhibitor) vs. normalized response - Variable slope.

Authentic virus neutralization assay

Purified BD55-1205 is subsequently diluted in two-fold (from 500 ng/mL to 0.244 ng/mL). These

670 diluted antibodies were mixed with live virus suspension (SARS-CoV-2 WT (Wuhan-Hu-1), BA.1

bioRxiv preprint doi: https://doi.org/10.1101/2024.04.16.589454; this version posted April 18, 2024. The copyright holder for this preprint (which was not certified by peer review) is the author/funder, who has granted bioRxiv a license to display the preprint in perpetuity. It is made available under aCC-BY-NC-ND 4.0 International license.

(EPI_ISL_8187354), BA.5.2.1 (EPI_ISL_17261619.2), FL.8 (XBB.1.9.1.8, EPI_ISL_17262369) containing 100 cell culture infectious dose 50% ($CCID_{50}$) and added to 96-well plates at a 1:1 ratio. The plates were incubated in a 36.5 °C incubator with 5% CO_2 for 2 h. Following the incubation, Vero cells (a gift from WHO, (ATCC, CCL-81)) were added to each well containing the antibody-
675 virus mixture. The plates were further incubated for 5 days in an incubator with 5% CO_2 at 36.5 °C. Cytopathic effects were evaluated by microscopy, and the IC_{50} values were determined by fitting two-parameter Hill equations. Experiments were conducted in four biological replicates in a biosafety level 3 (BSL-3) facility.

680 **Preparation of spike-pseudotyped rVSV**

Similar to previous reports, SARS-CoV-2 XBB.1.5 S-pseudotyped rVSV was constructed and rescued from DNA clones [43,64]. In brief, the VSV G gene on the plasmid encoding VSV anti-genome with T7 promoter was replaced by codon-optimized SARS-CoV-2 XBB.1.5 Spike gene with a C-terminal 21-aa deletion. GFP reporter gene was inserted into the VSV genome before the Spike gene.
685 BHK21 cells were infected with the vaccinia virus vTF7-3 that expresses T7 polymerase for 2 hours, and the supernatant was discarded. The VSV antigenome plasmid, and helper plasmids encoding VSV N, P, G, and L genes (Kerafast, EH1013-1016) were co-transfected to the cells using Lipofectamine 300. After 48-hour incubation, the supernatant was collected, filtered by a 0.22 µm filter, and passaged in Vero E6 cells. The virus was passaged every 2-3 days. After 3-4 times
690 amplification, the viral RNA was extracted and amplified by reverse transcription PCR. The Spike gene was then amplified and sequenced for validation. The supernatant that contains the rescued virus was aliquoted and stored at -80°C.

rVSV-based escape mutation screening under antibody pressure

695 Monoclonal antibodies were prepared at concentrations of 5, 1.25, 0.3125, and 0.078 µg/mL in Dulbecco's Modified Eagle Medium (DMEM) supplemented with 2% fetal bovine serum (FBS). In some replicates, an additional concentration of 20 µg/mL was also included. A volume of 0.5 mL of each dilution was added to individual wells of a 24-well plate. Subsequently, 0.5 mL of XBB.1.5-S-pseudotyped recombinant vesicular stomatitis virus (rVSV) with a titer of 4×10^6 focus-forming

bioRxiv preprint doi: https://doi.org/10.1101/2024.04.16.589454; this version posted April 18, 2024. The copyright holder for this preprint (which was not certified by peer review) is the author/funder, who has granted bioRxiv a license to display the preprint in perpetuity. It is made available under aCC-BY-NC-ND 4.0 International license.

700 units per mL (FFU/mL) was introduced to each well, resulting in a total volume of 1 mL per well. The plates were incubated at room temperature for 30 minutes to allow antibody-virus binding. After incubation, 200 μL of Vero cell suspension (1×10^6 cells/mL) was added to each well, bringing the final volume to 1.2 mL. The cell-virus-antibody mixture was then cultured at 37°C in an atmosphere containing 5% CO_2 for 72 hours. The fluorescence signal, indicating successful viral
705 entry and replication, was captured using a BioTek Cytation 5 Cell Imaging Multimode Reader (Agilent).

For the viral passage experiment, the supernatants from GFP-positive wells that contained the highest concentration of antibodies were harvested. The samples were centrifuged at 350 g for 3 minutes, and the clarified supernatants were then diluted in DMEM supplemented with 2% FBS,
710 and mixed with antibodies at various concentrations and incubated for 30 minutes before the addition of Vero cells. Subsequent passages were performed under identical conditions to those of the initial experiment, until the virus could successfully infected cells (GFP^+) under the pressure of antibody at the highest concentration.

715 **Recombinant RBD expression and purification**

DNA fragments that encode SARS-CoV-2 variant RBD (Spike 319-541) were codon-optimized for human cell expression and synthesized by Genscript. His-AVI tags were added at the end of the RBD gene fragments. The fragments were then inserted into pCMV3 vectors through infusion (Vazyme). The recombination products were transformed into E. coli DH5α competent cells
720 (Tsingke). Colonies with the desired plasmids were confirmed by Sanger sequencing (Azenta) and cultured for plasmid extraction (CWBIO). 293F cells were transfected with the constructed plasmids and cultured for 6 days. The products were purified using Ni-NTA columns (Changzhou Smart-lifesciences, SA005100) and the purified samples were verified by SDS-PAGE.

725 **Surface plasmon resonance**

SPR experiments were performed on Biacore 8K (Cytiva). mAbs (human IgG1) were immobilized onto Protein A sensor chips (Cytiva). Purified SARS-CoV-2 variant RBDs were prepared in serial dilutions (6.25, 12.5, 25, 50, and 100nM) and injected over the sensor chips. The response units

bioRxiv preprint doi: https://doi.org/10.1101/2024.04.16.589454; this version posted April 18, 2024. The copyright holder for this preprint (which was not certified by peer review) is the author/funder, who has granted bioRxiv a license to display the preprint in perpetuity. It is made available under aCC-BY-NC-ND 4.0 International license.

were recorded by Biacore 8K Evaluation Software 3.0 (Cytiva) at room temperature, and the raw
730 data curves were fitted to a 1:1 binding model to determine the affinities (K_D) using Biacore 8K Evaluation Software 3.0 (Cytiva).

Protein expression and purification for Cryo-EM

The Spike gene of XBB.1.5 (T19I, Δ24-26, A27S, V83A, G142D, Δ144, H146Q, Q183E, V213E,
735 G252V, G339H, R346T, L368I, S371F, S373P, S375F, T376A, D405N, R408S, K417N, N440K, V445P, G446S, N460K, S477N, T478K, E484A, F486P, F490S, R493Q, Q498R, N501Y, Y505H, D614G, H655Y, N679K, P681H, N764K, D796Y, Q954H, N969K) and XBB.1.5 RBD were realized by overlapping PCR with the full-length S gene (residues 1-1208, GenBank: MN908947) as template. The S gene was constructed into the vector pCAGGS with a T4 fibrin trimerization
740 motif and a HRV3C protease site and a Twin-Strep-tag at the C-terminal of spike and RBD sequences to facilitate protein purification and was mutated as previously described [65]. All the constructed vector were transiently transfected into suspended HEK293F cells and cultured at 37 ˚C in a rotating, humidified incubator supplied with 8% CO2 and maintained at 130 rpm. After incubation for 72h, the supernatant was harvested, concentrated, and exchanged into the binding
745 buffer by tangential flow filtration cassette. The S proteins were then separated by chromatography using resin attached with streptavidin and further purified by size exclusion chromatography using a Superose 6 10/300(GE Healthcare) in 20 mM Tris, 200mM NaCl, pH 8.0.

Production of Fab fragment

750 To generate the Fab fragments for Cryo-EM analyses, the purified antibodies were processed using the Pierce FAB preparation kit (Thermo Scientific) as described previously [18]. Briefly, the samples were first applied to desalination columns to remove the salt. After centrifugation, the flow through was collected and incubated with beads attached with papain to cleave Fab fragments from the whole antibodies. Then the mixtures were transferred to Protein A affinity column which specifically binds
755 the Fc fragments of antibodies. After centrifugation, the Fab fragments were obtained and dialyzed into Phosphate Buffered Saline (PBS).

bioRxiv preprint doi: https://doi.org/10.1101/2024.04.16.589454; this version posted April 18, 2024. The copyright holder for this preprint (which was not certified by peer review) is the author/funder, who has granted bioRxiv a license to display the preprint in perpetuity. It is made available under aCC-BY-NC-ND 4.0 International license.

Cryo-EM sample collection, data acquisition and structure determination

The cryo-EM samples of S trimers in complex with BD55-1205 with a molar ratio of 1:4 (S
760 protein:BD55-1205) on ice to obtain S-BD55-1205 complex. Then, the complex was deposited onto the freshly glow-discharged grids (C-flat 1.2/1.3 Au). After 6 seconds' blotting in 100% relative humidity, the grid was plunged into liquid ethane automatically by Vitrobot (FEI). Cryo-EM data sets were collected at a 200 kV FEI Talos Arctica microscope equipped with a K2 detector. Movies (32 frames, each 0.2 s, total dose of 60 e/Å^{-2}) were recorded with a defocus range between 1.5-2.7
765 μm. Automated single particle data acquisition was carried out by SerialEM, with a calibrated magnification of 75,000, yielding a final pixel size of 1.04 Å. A total of 5722 micrographs were collected. CryoSPARC was used to correct beam induced motion and average frames. Then, the defocus value of each micrograph was estimated by patch CTF estimation. 2515383 particles of XBB.1.5 S-BD55-1205 complex were autopicked and extracted for further 2D classification and
770 hetero-refinement. After that, 238788 particles of XBB.1.5 S-BD55-1205 complex were used for homo-refinement in cryoSPARC for the final cryo-EM density.

To improve the resolution of the binding surface of RBD-antibody, the cryo-EM sample of XBB.1.5 RBD in complex with BD55-1205 and BD57-0120 Fab, which is another RBD-targeting mAb that doesn't compete with BD55-1205, was also deposited. This approach allowed us to deduce a more
775 accurate epitope and paratope than was achievable using the flexible up RBD conformation in the BD55-1205-S cryo-EM structure, with BD57-0120 Fab utilized to increase the molecular weight of the complex. We performed asymmetric reconstruction of the complex structure, achieving an overall resolution of 3.3 Å, enabling reliable analysis of the interaction interface.The cryo-EM samples of XBB.1.5 RBD in complex with BD55-1205 were mixed in a molar ratio of 1:1.2:1.2
780 (RDB: BD55-1205: BD57-0120). Movies (32 frames, each 0.2 s, total dose of 60 e /Å^{-2}) were recorded using a Falcon 4 Summit direct detector with a defocus range between 1.5- 2.7 μm. Automated single particle data acquisition was carried out by EPU, with a calibrated magnification of 96,000, yielding a final pixel size of 0.808 Å. A total of 5866 micrographs for XBB.1.5 RBD-BD55-1205/BD57-0120 complex were collected. CryoSPARC was used to correct beam induced

bioRxiv preprint doi: https://doi.org/10.1101/2024.04.16.589454; this version posted April 18, 2024. The copyright holder for this preprint (which was not certified by peer review) is the author/funder, who has granted bioRxiv a license to display the preprint in perpetuity. It is made available under aCC-BY-NC-ND 4.0 International license.

785 motion and average frames. Then, the defocus value of each micrograph was estimated by patch CTF estimation. 3186044 particles of XBB.1.5 RBD-BD55-1205/ BD57-0120 complex were autopicked and extracted for further 2D classification and hetero-refinement. After that, 266321 particles of XBB.1.5 RBD-BD55-1205/BD57-0120 complex were used for homo-refinement and non-uniform refinement in cryoSPARC for the final cryo-EM density.

790 The resolutions were evaluated on the basis of the gold-standard Fourier shell correction (threshold = 0.143) and evaluated by ResMap. All dataset processing is shown in the Extended Data Fig. 6.

Structure model fitting and refinement

The atom models of the complex were first fitting the chain of the apo (PDB: 7XNQ) and Fab
795 (predicted by AlphaFold) into the obtained cryo-EM density by Chimera. Then the structure was manually adjusted and corrected according to the protein sequences and density in Coot, real-space refinement was performed by Phenix.

Generation of modified mRNA and LNPs

800 BD1205 with the 'LA' modification and CHKV-24 with the 'LS" modification (for consistency with histrocial data) were used in the studies. Sequence-optimized mRNA encoding functional IgG monoclonal antibodies were synthesized *in vitro* using an optimized T7 RNA polymerase-mediated transcription reaction with complete replacement of uridine by N1-methyl-pseudouridine [66]. The reactions included a DNA template containing an open reading frame flanked by 5′ untranslated
805 region (UTR) and 3′ UTR sequences with a terminal encoded polyA tail. Free mRNA was purified, buffer exchanged and sterile filtered.

Lipid nanoparticle-formulated mRNA was produced through a modified ethanol-drop nanoprecipitation process as described previously [67]. Briefly, ionizable, structural, helper, and polyethylene glycol lipids were mixed with mRNA in acetate buffe at a pH of 5.0 and at a ratio of
810 3:1 (lipids:mRNA). The mixture was neutralized with Tris-Cl at a pH 7.5, sucrose was added as a cryoprotectant, and the final solution was sterile filtered. Vials were filled with formulated LNP and

bioRxiv preprint doi: https://doi.org/10.1101/2024.04.16.589454; this version posted April 18, 2024. The copyright holder for this preprint (which was not certified by peer review) is the author/funder, who has granted bioRxiv a license to display the preprint in perpetuity. It is made available under aCC-BY-NC-ND 4.0 International license.

stored frozen at –70°C until further use. The drug product underwent analytical characterization, which included the determination of particle size and polydispersity, encapsulation, mRNA purity, osmolality, pH, endotoxin and bioburden, and the material was deemed acceptable for *in vivo* study.

815

Expression of mAbs in mice

Homozygous 'Tg32-SCID' mice (B6.Cg-Fcgrt^{tm1Dcr} Prkdcscid Tg(FCGRT)32Dcr/DcrJ cat. no. 018441) and 'Tg32' mice (B6.Cg-Fcgrt^{tm1Dcr} Tg(FCGRT)32Dcr/Dry, cat. no. 014565) were obtained from The Jackson Laboratory, Bar Harbour, Maine. Animals were housed in groups of 4, fed
820 standard chow diets, subjected to a photoperiod of 12 hours on, 12 hours off dark/light cycle and kept at an ambient animal room temperature of 70° ± 2° F with a room humidity of 50% ± 5%.

Six- to 8-week-old male and female Tg32-SCID mice (The Jackson Laboratory) or male and female Tg32 mice (The Jackson Laboratory) in groups of 4, were injected intravenously with the indicated mRNA LNP, at the indicated dose in 100 µL. All mRNA LNPs for *in vivo* were prepared by
825 coformulations of HC and LC for the expression of the full IgG. Mice were bled via submandibular vein at the indicated time points and serum was isolated for antibody quantification by ELISA and assessment of serum neutralizing titer. At the final indicated time point, mice were euthanized via CO_2 asphyxiation and a terminal bleed was collected via cardiac puncture.

All animal experiments were carried out in compliance with an approved Institutional Animal Care
830 and Use Committee (IACUC) protocol. Moderna's IACUC requires adherence to the standards of animal care laid out in the *Guide for the Care and Use of Laboratory Animals* of the National Institutes of Health. Experiments were neither randomized nor blinded.

Mouse serum ELISA for human IgG quantification

835 To quantitate total human IgG (hIgG), 96-well NUNC Maxisorp plates (ThermoScientific, 439454) were coated with 0.1 mL per well of goat anti-human IgG Fc fragment (Bethyl A80-104A) at 1:100 dilution in 0.05 M carbonate-bicarbonate (Sigma C30411) overnight at 4°C. Plates were washed with an automated plate washer (Biotek) 4x with 0.05% PBS-T and were subsequently blocked with

bioRxiv preprint doi: https://doi.org/10.1101/2024.04.16.589454; this version posted April 18, 2024. The copyright holder for this preprint (which was not certified by peer review) is the author/funder, who has granted bioRxiv a license to display the preprint in perpetuity. It is made available under aCC-BY-NC-ND 4.0 International license.

0.2 mL per well of Superblock PBST (ThermoFisher, 37515) for 1.5 hour at 37°C. Using purified
840 antibodies as a standard, mRNA transfection supernatant or mouse serum was serially diluted in PBST in a dilution plate and 0.1mL per well was transferred to the coated plates and incubated for 2 hour at 37°C. Following incubation, plates were subsequently washed and incubated with 0.1 mL per well of goat anti-human IgG horseradish peroxidase (HRP; Southern Biotech; 2030-05, 1:5000), for 1 hour at 37°C. Plates were subsequently washed and incubated with 0.1 mL per well
845 of Sureblue TMB 1-C substrate (Sera care, 52-00-04) for 10 minutes. The reaction was stopped with 0.1 mL per well of TMB Stop solution (SeraCare, 50-85-05) and read at an absorbance of 450nm on a SpectraMax ABS Microplate Reader (Molecular Devices). Absolute quantities of human antibody in transfection supernatant or mouse serum were extrapolated in GraphPad Prism 9 using a standard curve.

850

Mice serum pseudovirus neutralization assays

Codon-optimized full-length spike genes (XBB.1.5, JN.1 and HK.3.1) were cloned into a pCAGGS vector. Spike genes contained the following mutations: (a) XBB.1.5: T19I, L24-, P25-, P26-, A27S, V83A, G142D, Y144-, H146Q, Q183E, V213E, G252V, G339H, R346T, L368I, S371F, S373P,
855 S375F, T376A, D405N, R408S, K417N, N440K, V445P, G446S, N460K, S477N, T478K, E484A, F486P, F490S, Q498R, N501Y, Y505H, D614G, H655Y, N679K, P681H, N764K, D796Y, Q954H, N969K; (b) JN.1: ins16MPLF, T19I, R21T, L24-, P25-, P26-, A27S, S50L, H69-, V70-, V127F, G142D, Y144-, F157S, R158G, N211-, L212I, V213G, L216F, H245N, A264D, I332V, G339H, K356T, S371F, S373P, S375F, T376A, R403K, D405N, R408S, K417N, N440K, V445H, G446S,
860 N450D, L452W, L455S, N460K, S477N, T478K, N481K, V483-, E484K, F486P, Q498R, N501Y, Y505H, E554K, A570V, D614G, P621S, H655Y, N679K, P681R, N764K, D796Y, S939F, Q954H, N969K, P1143L; and (c) HK.3.1: T19I, L24-, P25-, P26-, A27S, Q52H, V83A, G142D, Y144-, H146Q, F157L, Q183E, V213E, G252V, G339H, R346T, L368I, S371F, S373P, S375F, T376A, D405N, R408S, K417N, N440K, V445P, G446S, L455F, F456L, N460K, S477N, T478K, E484A,
865 F486P, F490S, Q498R, N501Y, Y505H, D614G, H655Y, N679K, P681H, N764K, D796Y, Q954H, N969K. To generate VSVΔG-based SARS-CoV-2 pseudovirus, BHK-21/WI-2 cells were

bioRxiv preprint doi: https://doi.org/10.1101/2024.04.16.589454; this version posted April 18, 2024. The copyright holder for this preprint (which was not certified by peer review) is the author/funder, who has granted bioRxiv a license to display the preprint in perpetuity. It is made available under aCC-BY-NC-ND 4.0 International license.

transfected with the spike expression plasmid and infected by VSVΔG-firefly-luciferase as previously described [68]. VeroE6 cells were used as target cells for the neutralization assay and maintained in DMEM supplemented with 10% FBS. To perform neutralization assay, mouse serum
870 samples were heat-inactivated for 45 minutes at 56 °C, and serial dilutions were made in DMEM supplemented with 10% FBS. The diluted serum samples or culture medium (serving as virus-only control) were mixed with VSVΔG-based SARS-CoV-2 pseudovirus and incubated at 37 °C for 45 minutes. The inoculum virus or virus–serum mix was subsequently used to infect VeroE6 cells (ATCC, CRL-1586) for 18 hours at 37 °C. At 18 hours after infection, an equal volume of One-Glo
875 reagent (Promega, E6120) was added to culture medium for readout using a BMG PHERastar-FSX plate reader. The percentage of neutralization was calculated based on relative light units (RLUs) of the virus control and subsequently analyzed using four-parameter logistic curve (GraphPad Prism 8.0).

880 **References**

1 Sachs, J. D. *et al.* The Lancet Commission on lessons for the future from the COVID-19 pandemic. *Lancet* **400**, 1224-1280 (2022). https://doi.org:10.1016/S0140-6736(22)01585-9

2 Carabelli, A. M. *et al.* SARS-CoV-2 variant biology: immune escape, transmission and
885 fitness. *Nature Reviews Microbiology* **21**, 162-177 (2023). https://doi.org:10.1038/s41579-022-00841-7

3 Yang, S. *et al.* Fast evolution of SARS-CoV-2 BA.2.86 to JN.1 under heavy immune pressure. *Lancet Infect Dis* (2023). https://doi.org:10.1016/S1473-3099(23)00744-2

4 Yang, S. *et al.* Antigenicity and infectivity characterisation of SARS-CoV-2 BA.2.86. *The*
890 *Lancet Infectious Diseases* **23**, e457-e459 (2023). https://doi.org:10.1016/S1473-3099(23)00573-X

5 Kaku, Y. *et al.* Antiviral efficacy of the SARS-CoV-2 XBB breakthrough infection sera against omicron subvariants including EG.5. *The Lancet Infectious Diseases* **23**, e395-e396 (2023). https://doi.org:10.1016/S1473-3099(23)00553-4

895 6 Yamasoba, D. *et al.* Virological characteristics of the SARS-CoV-2 omicron XBB.1.16 variant. *The Lancet Infectious Diseases* **23**, 655-656 (2023). https://doi.org:10.1016/S1473-3099(23)00278-5

7 Faraone, J. N. *et al.* Immune Evasion and Membrane Fusion of SARS-CoV-2 XBB Subvariants EG.5.1 and XBB.2.3. *Emerg Microbes Infect*, 2270069 (2023).
900 https://doi.org:10.1080/22221751.2023.2270069

8 Jian, F. *et al.* Convergent evolution of SARS-CoV-2 XBB lineages on receptor-binding domain 455–456 synergistically enhances antibody evasion and ACE2 binding. *PLOS*

bioRxiv preprint doi: https://doi.org/10.1101/2024.04.16.589454; this version posted April 18, 2024. The copyright holder for this preprint (which was not certified by peer review) is the author/funder, who has granted bioRxiv a license to display the preprint in perpetuity. It is made available under aCC-BY-NC-ND 4.0 International license.

Pathogens **19**, e1011868 (2023). https://doi.org:10.1371/journal.ppat.1011868
9 Kaku, Y. *et al.* Virological characteristics of the SARS-CoV-2 JN.1 variant. *Lancet Infect Dis*
905 (2024). https://doi.org:10.1016/S1473-3099(23)00813-7
10 Jeworowski, L. M. *et al.* Humoral immune escape by current SARS-CoV-2 variants BA.2.86 and JN.1, December 2023. *Eurosurveillance* **29**, 2300740 (2024). https://doi.org:doi:https://doi.org/10.2807/1560-7917.ES.2024.29.2.2300740
11 Wang, Q. *et al.* XBB.1.5 monovalent mRNA vaccine booster elicits robust neutralizing
910 antibodies against emerging SARS-CoV-2 variants. *bioRxiv*, 2023.2011.2026.568730 (2023). https://doi.org:10.1101/2023.11.26.568730
12 Dougan, M. *et al.* Bamlanivimab plus Etesevimab in Mild or Moderate Covid-19. *N Engl J Med* **385**, 1382-1392 (2021). https://doi.org:10.1056/NEJMoa2102685
13 Klasse, P. J. & Moore, J. P. Antibodies to SARS-CoV-2 and their potential for therapeutic
915 passive immunization. *eLife* **9**, e57877 (2020). https://doi.org:10.7554/eLife.57877
14 Gupta, A. *et al.* Early Treatment for Covid-19 with SARS-CoV-2 Neutralizing Antibody Sotrovimab. *New England Journal of Medicine* **385**, 1941-1950 (2021). https://doi.org:10.1056/NEJMoa2107934
15 Weinreich, D. M. *et al.* REGN-COV2, a Neutralizing Antibody Cocktail, in Outpatients with
920 Covid-19. *New England Journal of Medicine* **384**, 238-251 (2020). https://doi.org:10.1056/NEJMoa2035002
16 Kelley, B. Developing therapeutic monoclonal antibodies at pandemic pace. *Nature Biotechnology* **38**, 540-545 (2020). https://doi.org:10.1038/s41587-020-0512-5
17 Bruel, T. *et al.* Serum neutralization of SARS-CoV-2 Omicron sublineages BA.1 and BA.2
925 in patients receiving monoclonal antibodies. *Nat Med* **28**, 1297-1302 (2022). https://doi.org:10.1038/s41591-022-01792-5
18 Cao, Y. *et al.* Omicron escapes the majority of existing SARS-CoV-2 neutralizing antibodies. *Nature* **602**, 657-663 (2022). https://doi.org:10.1038/s41586-021-04385-3
19 Cao, Y. *et al.* BA.2.12.1, BA.4 and BA.5 escape antibodies elicited by Omicron infection.
930 *Nature* **608**, 593-602 (2022). https://doi.org:10.1038/s41586-022-04980-y
20 Iketani, S. *et al.* Antibody evasion properties of SARS-CoV-2 Omicron sublineages. *Nature* **604**, 553-556 (2022). https://doi.org:10.1038/s41586-022-04594-4
21 Cox, M. *et al.* SARS-CoV-2 variant evasion of monoclonal antibodies based on in vitro studies. *Nature Reviews Microbiology* **21**, 112-124 (2023).
935 https://doi.org:10.1038/s41579-022-00809-7
22 Cameroni, E. *et al.* Broadly neutralizing antibodies overcome SARS-CoV-2 Omicron antigenic shift. *Nature* **602**, 664-670 (2022). https://doi.org:10.1038/s41586-021-04386-2
23 Park, Y. J. *et al.* Antibody-mediated broad sarbecovirus neutralization through ACE2
940 molecular mimicry. *Science* **375**, 449-454 (2022). https://doi.org:10.1126/science.abm8143
24 Luo, S. *et al.* An Antibody from Single Human VH-rearranging Mouse Neutralizes All SARS-CoV-2 Variants Through BA.5 by Inhibiting Membrane Fusion. *Sci Immunol* **0**, eadd5446 (2022). https://doi.org:10.1126/sciimmunol.add5446
945 25 Nutalai, R. *et al.* Potent cross-reactive antibodies following Omicron breakthrough in vaccinees. *Cell* **185**, 2116-2131 e2118 (2022). https://doi.org:10.1016/j.cell.2022.05.014

bioRxiv preprint doi: https://doi.org/10.1101/2024.04.16.589454; this version posted April 18, 2024. The copyright holder for this preprint (which was not certified by peer review) is the author/funder, who has granted bioRxiv a license to display the preprint in perpetuity. It is made available under aCC-BY-NC-ND 4.0 International license.

26 Hong, Q. *et al.* Molecular basis of receptor binding and antibody neutralization of Omicron. *Nature* **604**, 546-552 (2022). https://doi.org:10.1038/s41586-022-04581-9

27 Westendorf, K. *et al.* LY-CoV1404 (bebtelovimab) potently neutralizes SARS-CoV-2
950 variants. *Cell Rep* **39**, 110812 (2022). https://doi.org:10.1016/j.celrep.2022.110812

28 Bianchini, F. *et al.* Human neutralizing antibodies to cold linear epitopes and subdomain 1 of the SARS-CoV-2 spike glycoprotein. *Science Immunology* **8**, eade0958 (2023). https://doi.org:doi:10.1126/sciimmunol.ade0958

29 Liu, L. *et al.* Antibodies targeting a quaternary site on SARS-CoV-2 spike glycoprotein
955 prevent viral receptor engagement by conformational locking. *Immunity* **56**, 2442-2455.e2448 (2023). https://doi.org:https://doi.org/10.1016/j.immuni.2023.09.003

30 Cao, Y. *et al.* Imprinted SARS-CoV-2 humoral immunity induces convergent Omicron RBD evolution. *Nature* **614**, 521-529 (2023). https://doi.org:10.1038/s41586-022-05644-7

31 Li, G., Hilgenfeld, R., Whitley, R. & De Clercq, E. Therapeutic strategies for COVID-19:
960 progress and lessons learned. *Nature Reviews Drug Discovery* **22**, 449-475 (2023). https://doi.org:10.1038/s41573-023-00672-y

32 Yisimayi, A. *et al.* Repeated Omicron exposures override ancestral SARS-CoV-2 immune imprinting. *Nature* **625**, 148-156 (2024). https://doi.org:10.1038/s41586-023-06753-7

33 Cao, Y. *et al.* Rational identification of potent and broad sarbecovirus-neutralizing
965 antibody cocktails from SARS convalescents. *Cell Rep* **41**, 111845 (2022). https://doi.org:10.1016/j.celrep.2022.111845

34 Cao, Y. *et al.* Potent Neutralizing Antibodies against SARS-CoV-2 Identified by High-Throughput Single-Cell Sequencing of Convalescent Patients' B Cells. *Cell* **182**, 73-84 e16 (2020). https://doi.org:10.1016/j.cell.2020.05.025

970 35 Du, S. *et al.* Structures of SARS-CoV-2 B.1.351 neutralizing antibodies provide insights into cocktail design against concerning variants. *Cell Res* **31**, 1130-1133 (2021). https://doi.org:10.1038/s41422-021-00555-0

36 Cao, Y. *et al.* Humoral immune response to circulating SARS-CoV-2 variants elicited by inactivated and RBD-subunit vaccines. *Cell Res* **31**, 732-741 (2021).
975 https://doi.org:10.1038/s41422-021-00514-9

37 Du, S. *et al.* Structurally Resolved SARS-CoV-2 Antibody Shows High Efficacy in Severely Infected Hamsters and Provides a Potent Cocktail Pairing Strategy. *Cell* **183**, 1013-1023 e1013 (2020). https://doi.org:10.1016/j.cell.2020.09.035

38 Tan, C.-W. *et al.* Pan-Sarbecovirus Neutralizing Antibodies in BNT162b2-Immunized
980 SARS-CoV-1 Survivors. *New England Journal of Medicine* **385**, 1401-1406 (2021). https://doi.org:10.1056/NEJMoa2108453

39 Ju, B. *et al.* Infection with wild-type SARS-CoV-2 elicits broadly neutralizing and protective antibodies against omicron subvariants. *Nature Immunology* **24**, 690-699 (2023). https://doi.org:10.1038/s41590-023-01449-6

985 40 Li, L. *et al.* Breakthrough infection elicits hypermutated IGHV3-53/3-66 public antibodies with broad and potent neutralizing activity against SARS-CoV-2 variants including the emerging EG.5 lineages. *PLOS Pathogens* **19**, e1011856 (2023). https://doi.org:10.1371/journal.ppat.1011856

41 Chen, Y. *et al.* Broadly neutralizing antibodies to SARS-CoV-2 and other human
990 coronaviruses. *Nature Reviews Immunology* **23**, 189-199 (2023).

bioRxiv preprint doi: https://doi.org/10.1101/2024.04.16.589454; this version posted April 18, 2024. The copyright holder for this preprint (which was not certified by peer review) is the author/funder, who has granted bioRxiv a license to display the preprint in perpetuity. It is made available under aCC-BY-NC-ND 4.0 International license.

https://doi.org:10.1038/s41577-022-00784-3

42 Li, H. *et al.* Establishment of replication-competent vesicular stomatitis virus-based recombinant viruses suitable for SARS-CoV-2 entry and neutralization assays. *Emerg Microbes Infect* **9**, 2269-2277 (2020). https://doi.org:10.1080/22221751.2020.1830715

995 43 Wu, X. *et al.* Development of a Bioluminescent Imaging Mouse Model for SARS-CoV-2 Infection Based on a Pseudovirus System. *Vaccines* **11**, 1133 (2023).

44 Schmidt, F. *et al.* High genetic barrier to SARS-CoV-2 polyclonal neutralizing antibody escape. *Nature* **600**, 512-516 (2021). https://doi.org:10.1038/s41586-021-04005-0

45 Barnes, C. O. *et al.* SARS-CoV-2 neutralizing antibody structures inform therapeutic
1000 strategies. *Nature* **588**, 682-687 (2020). https://doi.org:10.1038/s41586-020-2852-1

46 Taylor, A. L. & Starr, T. N. Deep mutational scans of XBB.1.5 and BQ.1.1 reveal ongoing epistatic drift during SARS-CoV-2 evolution. *PLOS Pathogens* **19**, e1011901 (2023). https://doi.org:10.1371/journal.ppat.1011901

47 Yuan, M. *et al.* Structural basis of a shared antibody response to SARS-CoV-2. *Science*
1005 **369**, 1119-1123 (2020). https://doi.org:doi:10.1126/science.abd2321

48 Zemlin, M. *et al.* Expressed Murine and Human CDR-H3 Intervals of Equal Length Exhibit Distinct Repertoires that Differ in their Amino Acid Composition and Predicted Range of Structures. *Journal of Molecular Biology* **334**, 733-749 (2003). https://doi.org:https://doi.org/10.1016/j.jmb.2003.10.007

1010 49 Tuekprakhon, A. *et al.* Antibody escape of SARS-CoV-2 Omicron BA.4 and BA.5 from vaccine and BA.1 serum. *Cell* **185**, 2422-2433 e2413 (2022). https://doi.org:10.1016/j.cell.2022.06.005

50 Copin, R. *et al.* The monoclonal antibody combination REGEN-COV protects against SARS-CoV-2 mutational escape in preclinical and human studies. *Cell* **184**, 3949-3961
1015 e3911 (2021). https://doi.org:10.1016/j.cell.2021.06.002

51 Loo, Y. M. *et al.* The SARS-CoV-2 monoclonal antibody combination, AZD7442, is protective in nonhuman primates and has an extended half-life in humans. *Sci Transl Med* **14**, eabl8124 (2022). https://doi.org:10.1126/scitranslmed.abl8124

52 Self, W. H. *et al.* Efficacy and safety of two neutralising monoclonal antibody therapies,
1020 sotrovimab and BRII-196 plus BRII-198, for adults hospitalised with COVID-19 (TICO): a randomised controlled trial. *Lancet Infectious Diseases* **22**, 622-635 (2022). https://doi.org:10.1016/S1473-3099(21)00751-9

53 Levin, M. J. *et al.* Intramuscular AZD7442 (Tixagevimab–Cilgavimab) for Prevention of Covid-19. *New England Journal of Medicine* **386**, 2188-2200 (2022).
1025 https://doi.org:10.1056/NEJMoa2116620

54 O'Brien, M. P. *et al.* Subcutaneous REGEN-COV Antibody Combination to Prevent Covid-19. *New England Journal of Medicine* **385**, 1184-1195 (2021). https://doi.org:10.1056/NEJMoa2109682

55 Ison, M. G. *et al.* Prevention of COVID-19 Following a Single Intramuscular Administration
1030 of Adintrevimab: Results From a Phase 2/3 Randomized, Double-Blind, Placebo-Controlled Trial (EVADE). *Open Forum Infectious Diseases* **10** (2023). https://doi.org:10.1093/ofid/ofad314

56 Schmidt, P. *et al.* Antibody-mediated protection against symptomatic COVID-19 can be achieved at low serum neutralizing titers. *Science Translational Medicine* **15**, eadg2783

bioRxiv preprint doi: https://doi.org/10.1101/2024.04.16.589454; this version posted April 18, 2024. The copyright holder for this preprint (which was not certified by peer review) is the author/funder, who has granted bioRxiv a license to display the preprint in perpetuity. It is made available under aCC-BY-NC-ND 4.0 International license.

1035 (2023). https://doi.org:doi:10.1126/scitranslmed.adg2783

57 Roopenian, D. C., Christianson, G. J. & Sproule, T. J. in *Mouse Models for Drug Discovery: Methods and Protocols* (eds Gabriele Proetzel & Michael V. Wiles) 93-104 (Humana Press, 2010).

58 August, A. *et al.* A phase 1 trial of lipid-encapsulated mRNA encoding a monoclonal
1040 antibody with neutralizing activity against Chikungunya virus. *Nature Medicine* **27**, 2224-2233 (2021). https://doi.org:10.1038/s41591-021-01573-6

59 Kose, N. *et al.* A lipid-encapsulated mRNA encoding a potently neutralizing human monoclonal antibody protects against chikungunya infection. *Science Immunology* **4**, eaaw6647 (2019). https://doi.org:doi:10.1126/sciimmunol.aaw6647

1045 60 Nie, J. *et al.* Establishment and validation of a pseudovirus neutralization assay for SARS-CoV-2. *Emerg Microbes Infect* **9**, 680-686 (2020). https://doi.org:10.1080/22221751.2020.1743767

61 Andreano, E. *et al.* SARS-CoV-2 escape from a highly neutralizing COVID-19 convalescent plasma. *Proceedings of the National Academy of Sciences* **118**, e2103154118 (2021).
1050 https://doi.org:doi:10.1073/pnas.2103154118

62 REED, L. J. & MUENCH, H. A SIMPLE METHOD OF ESTIMATING FIFTY PER CENT ENDPOINTS12. *American Journal of Epidemiology* **27**, 493-497 (1938). https://doi.org:10.1093/oxfordjournals.aje.a118408

63 Brai, A. *et al.* Exploring the Implication of DDX3X in DENV Infection: Discovery of the First-
1055 in-Class DDX3X Fluorescent Inhibitor. *ACS Medicinal Chemistry Letters* **11**, 956-962 (2020). https://doi.org:10.1021/acsmedchemlett.9b00681

64 Lawson, N. D., Stillman, E. A., Whitt, M. A. & Rose, J. K. Recombinant vesicular stomatitis viruses from DNA. *Proceedings of the National Academy of Sciences* **92**, 4477-4481 (1995). https://doi.org:doi:10.1073/pnas.92.10.4477

1060 65 Cui, Z. *et al.* Structural and functional characterizations of infectivity and immune evasion of SARS-CoV-2 Omicron. *Cell* **185**, 860-871 e813 (2022). https://doi.org:10.1016/j.cell.2022.01.019

66 Nelson, J. *et al.* Impact of mRNA chemistry and manufacturing process on innate immune activation. *Science Advances* **6**, eaaz6893 (2020).
1065 https://doi.org:doi:10.1126/sciadv.aaz6893

67 Sabnis, S. *et al.* A Novel Amino Lipid Series for mRNA Delivery: Improved Endosomal Escape and Sustained Pharmacology and Safety in Non-human Primates. *Molecular Therapy* **26**, 1509-1519 (2018). https://doi.org:https://doi.org/10.1016/j.ymthe.2018.03.010

1070 68 Whitt, M. A. Generation of VSV pseudotypes using recombinant ΔG-VSV for studies on virus entry, identification of entry inhibitors, and immune responses to vaccines. *Journal of Virological Methods* **169**, 365-374 (2010). https://doi.org:https://doi.org/10.1016/j.jviromet.2010.08.006

bioRxiv preprint doi: https://doi.org/10.1101/2024.04.16.589454; this version posted April 18, 2024. The copyright holder for this preprint (which was not certified by peer review) is the author/funder, who has granted bioRxiv a license to display the preprint in perpetuity. It is made available under aCC-BY-NC-ND 4.0 International license.

Figure 1

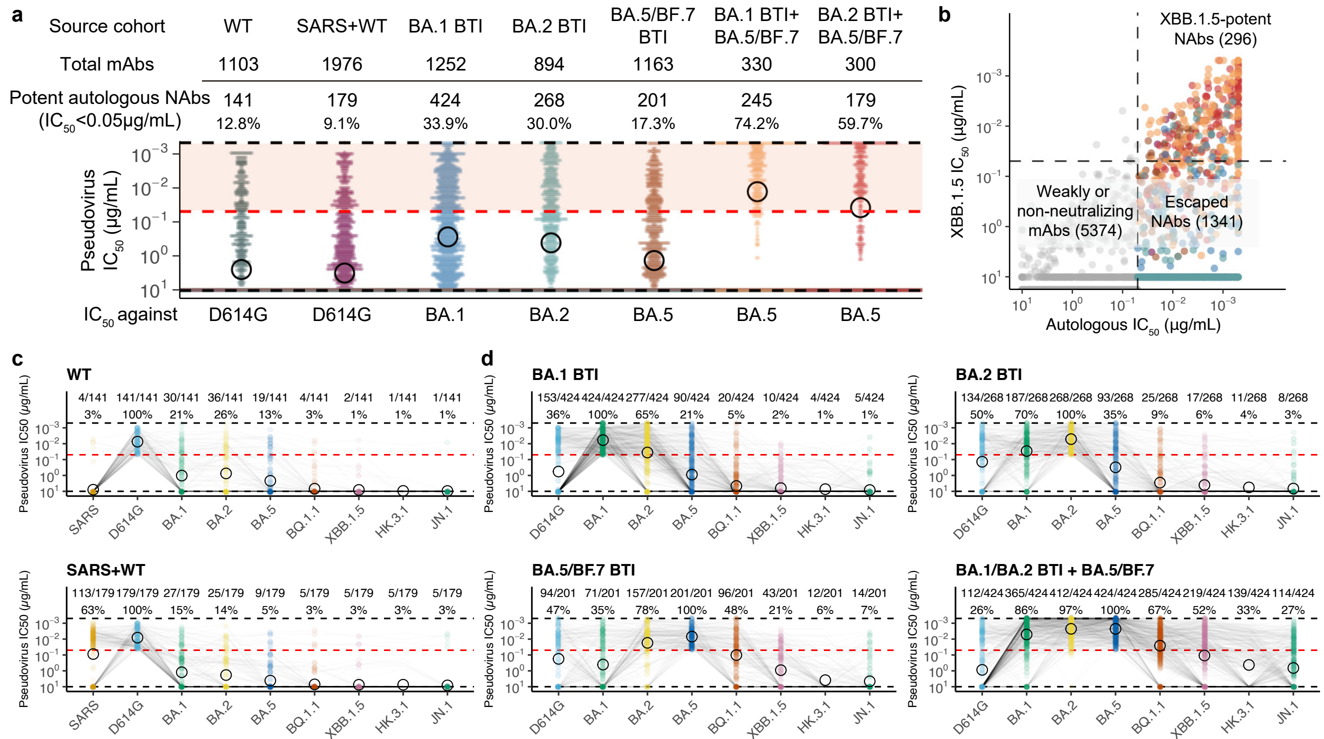

Figure 1 | Neutralization activities of RBD-targeting mAbs against SARS-CoV-2 variants
a, Neutralization of the 7,018 mAbs from individuals of 7 different immune histories against their corresponding last-exposure variant (autologous neutralization activity). Numbers and proportions of potent autologous NAbs (IC50 < 0.05 μg/mL) are annotated above each group of points. The black circles indicate the geometric mean values of each group. b, Relationship between the autologous neutralization activities and XBB.1.5-neutralizing activities of the involved mAbs. c-d, Neutralization activities of potent autologous NAbs against variants. Numbers and proportions of potent NAbs against each variant (IC50 < 0.05 μg/mL) are annotated.

bioRxiv preprint doi: https://doi.org/10.1101/2024.04.16.589454; this version posted April 18, 2024. The copyright holder for this preprint (which was not certified by peer review) is the author/funder, who has granted bioRxiv a license to display the preprint in perpetuity. It is made available under aCC-BY-NC-ND 4.0 International license.

Figure 2

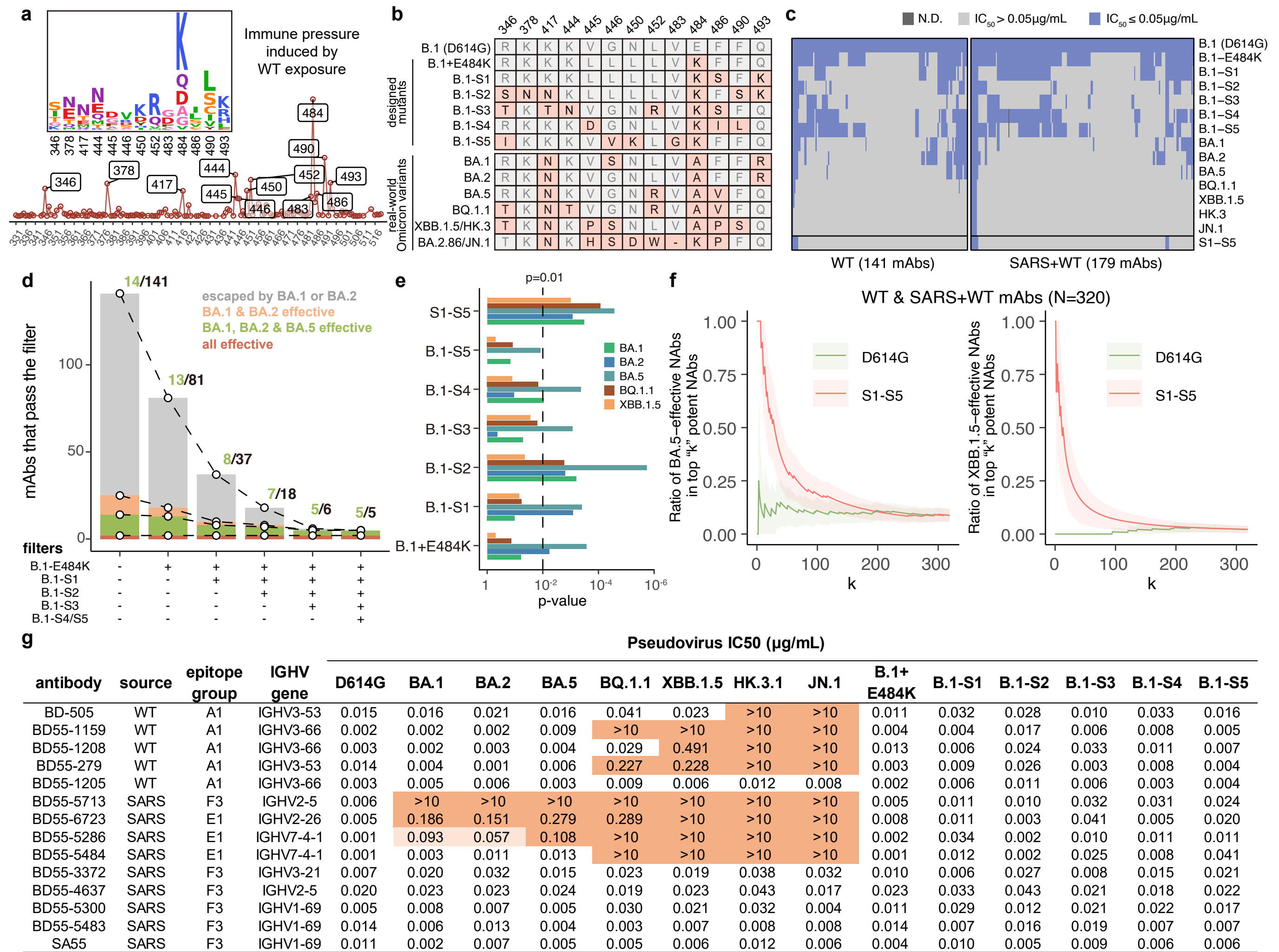

antibody	source	epitope group	IGHV gene	D614G	BA.1	BA.2	BA.5	BQ.1.1	XBB.1.5	HK.3.1	JN.1	B.1+ E484K	B.1-S1	B.1-S2	B.1-S3	B.1-S4	B.1-S5
BD-505	WT	A1	IGHV3-53	0.015	0.016	0.021	0.016	0.041	0.023	>10	>10	0.011	0.032	0.028	0.010	0.033	0.016
BD55-1159	WT	A1	IGHV3-66	0.002	0.002	0.002	0.009	>10	>10	>10	>10	0.004	0.004	0.017	0.006	0.008	0.005
BD55-1208	WT	A1	IGHV3-66	0.003	0.002	0.003	0.004	0.029	0.491	>10	>10	0.013	0.006	0.024	0.033	0.011	0.007
BD55-279	WT	A1	IGHV3-53	0.014	0.004	0.001	0.006	0.227	0.228	>10	>10	0.003	0.009	0.026	0.003	0.008	0.004
BD55-1205	WT	A1	IGHV3-66	0.003	0.005	0.006	0.003	0.009	0.006	0.012	0.008	0.002	0.006	0.011	0.006	0.003	0.004
BD55-5713	SARS	F3	IGHV2-5	0.006	>10	>10	>10	>10	>10	>10	>10	0.005	0.011	0.010	0.032	0.031	0.024
BD55-6723	SARS	E1	IGHV2-26	0.005	0.186	0.151	0.279	0.289	>10	>10	>10	0.008	0.011	0.003	0.041	0.005	0.020
BD55-5286	SARS	E1	IGHV7-4-1	0.001	0.093	0.057	0.108	>10	>10	>10	>10	0.002	0.034	0.002	0.010	0.011	0.011
BD55-5484	SARS	E1	IGHV7-4-1	0.001	0.003	0.011	0.013	>10	>10	>10	>10	0.001	0.012	0.002	0.025	0.008	0.041
BD55-3372	SARS	F3	IGHV3-21	0.007	0.020	0.032	0.015	0.023	0.019	0.038	0.032	0.010	0.006	0.027	0.008	0.015	0.021
BD55-4637	SARS	F3	IGHV2-5	0.020	0.023	0.023	0.024	0.019	0.023	0.043	0.017	0.023	0.033	0.043	0.021	0.018	0.022
BD55-5300	SARS	F3	IGHV1-69	0.005	0.008	0.007	0.005	0.030	0.021	0.032	0.004	0.011	0.029	0.012	0.021	0.022	0.017
BD55-5483	SARS	F3	IGHV1-69	0.014	0.006	0.013	0.004	0.003	0.007	0.008	0.008	0.014	0.007	0.016	0.019	0.007	0.007
SA55	SARS	F3	IGHV1-69	0.011	0.002	0.007	0.005	0.005	0.006	0.012	0.006	0.004	0.010	0.005	0.009	0.006	0.006

Figure 2 | Designed mutants based on mutation prediction defines bnAbs

a, Average escape profiles from DMS of mAbs (weighted by neutralization activities of each mAb against SARS-CoV-2 WT and the impact of each RBD mutation on ACE2 binding and RBD expression). b, Mutations harbored by the designed SARS-CoV-2 B.1-based mutants and real-world variants on the key sites indicated by DMS-based prediction. c, Neutralization capability of the mAbs from early cohorts (SARS+WT and WT) against the designed mutants and real-world Omicron variants. "S1-S5" indicates the highest IC50 against the five designed mutants. d, Number of NAbs from WT vaccinees or convalescents that pass the filter of designed mutants. Ratio of BA.1, BA.2, and BA.5-potent NAbs among the passed NAbs are annotated above the bar of each combination of filter. e, Significance for the enrichment of BA.1, BA.2, BA.5, BQ.1.1, or XBB.1.5-potent NAbs within NAbs that are from WT vaccinees or convalescents and pass each filter of designed mutants (hypergeometric test). f, Ratio of BA.5 or XBB.1.5-potent NAbs within the NAbs with "top k" neutralization activities against D614G or S1-S5. g, Information of the NAbs isolated from early cohorts that pass the designed filters.

bioRxiv preprint doi: https://doi.org/10.1101/2024.04.16.589454; this version posted April 18, 2024. The copyright holder for this preprint (which was not certified by peer review) is the author/funder, who has granted bioRxiv a license to display the preprint in perpetuity. It is made available under aCC-BY-NC-ND 4.0 International license.

Figure 3

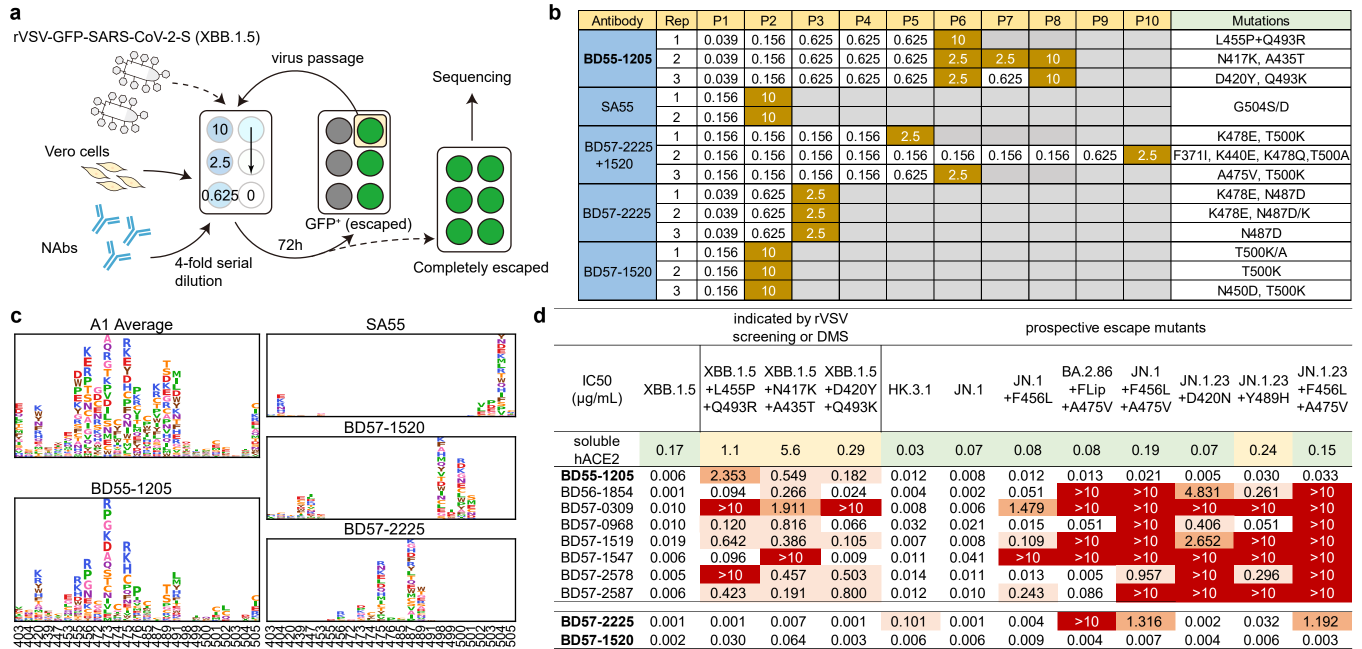

Antibody	Rep	P1	P2	P3	P4	P5	P6	P7	P8	P9	P10	Mutations
BD55-1205	1	0.039	0.156	0.625	0.625	0.625	10					L455P+Q493R
	2	0.039	0.156	0.625	0.625	0.625	2.5	2.5	10			N417K, A435T
	3	0.039	0.156	0.625	0.625	0.625	2.5	0.625	10			D420Y, Q493K
SA55	1	0.156	10									G504S/D
	2	0.156	10									
BD57-2225 +1520	1	0.156	0.156	0.156	0.156	2.5						K478E, T500K
	2	0.156	0.156	0.156	0.156	0.156	0.156	0.156	0.156	0.625	2.5	F371I, K440E, K478Q,T500A
	3	0.156	0.156	0.156	0.156	0.625	2.5					A475V, T500K
BD57-2225	1	0.039	0.625	2.5								K478E, N487D
	2	0.039	0.625	2.5								K478E, N487D/K
	3	0.039	0.625	2.5								N487D
BD57-1520	1	0.156	10									T500K/A
	2	0.156	10									T500K
	3	0.156	10									N450D, T500K

		indicated by rVSV screening or DMS			prospective escape mutants							
IC50 (μg/mL)	XBB.1.5	XBB.1.5 +L455P +Q493R	XBB.1.5 +N417K +A435T	XBB.1.5 +D420Y +Q493K	HK.3.1	JN.1	JN.1 +F456L	BA.2.86 +FLip +A475V	JN.1 +F456L +A475V	JN.1.23 +D420N	JN.1.23 +Y489H	JN.1.23 +F456L +A475V
soluble hACE2	0.17	1.1	5.6	0.29	0.03	0.07	0.08	0.08	0.19	0.07	0.24	0.15
BD55-1205	0.006	2.353	0.549	0.182	0.012	0.008	0.012	0.013	0.021	0.005	0.030	0.033
BD56-1854	0.001	0.094	0.266	0.024	0.004	0.002	0.051	>10	>10	4.831	0.261	>10
BD57-0309	0.010	>10	1.911	>10	0.008	0.006	1.479	>10	>10	>10	>10	>10
BD57-0968	0.010	0.120	0.816	0.066	0.032	0.021	0.015	0.051	>10	0.406	0.051	>10
BD57-1519	0.019	0.642	0.386	0.105	0.007	0.008	0.109	>10	>10	2.652	>10	>10
BD57-1547	0.006	0.096	>10	0.009	0.011	0.041	>10	>10	>10	>10	>10	>10
BD57-2578	0.005	>10	0.457	0.503	0.014	0.011	0.013	0.005	0.957	>10	0.296	>10
BD57-2587	0.006	0.423	0.191	0.800	0.012	0.010	0.243	0.086	>10	>10	>10	>10
BD57-2225	0.001	0.001	0.007	0.001	0.101	0.001	0.004	>10	1.316	0.002	0.032	1.192
BD57-1520	0.002	0.030	0.064	0.003	0.006	0.006	0.009	0.004	0.007	0.004	0.006	0.003

Figure 3 | BD55-1205 exhibits extraordinary resistance to escape mutations

a, Schematic for the rVSV-based escape mutation screening assays. b, Results of the escape screening by rVSV passaging under the pressure of NAbs. Values in the P1-P10 columns of the table indicates the highest concentration of NAb that was escaped by rVSV at the first passage to the tenth passage. The mutations of the final passage of rVSV determined by Sanger sequencing are annotated in the last column. c, DMS escape profiles (based on XBB.1.5 RBD) of the NAbs involved in the rVSV assays. The average profile of antibodies in epitope group A1 is also shown for comparison with BD55-1205. d, Neutralization of BD55-1205 and other NAbs against designed escape mutants according to rVSV screening and DMS profiles, and real-world emerging and prospective mutants with mutations on the epitope of BD55-1205.

bioRxiv preprint doi: https://doi.org/10.1101/2024.04.16.589454; this version posted April 18, 2024. The copyright holder for this preprint (which was not certified by peer review) is the author/funder, who has granted bioRxiv a license to display the preprint in perpetuity. It is made available under aCC-BY-NC-ND 4.0 International license.

Figure 4

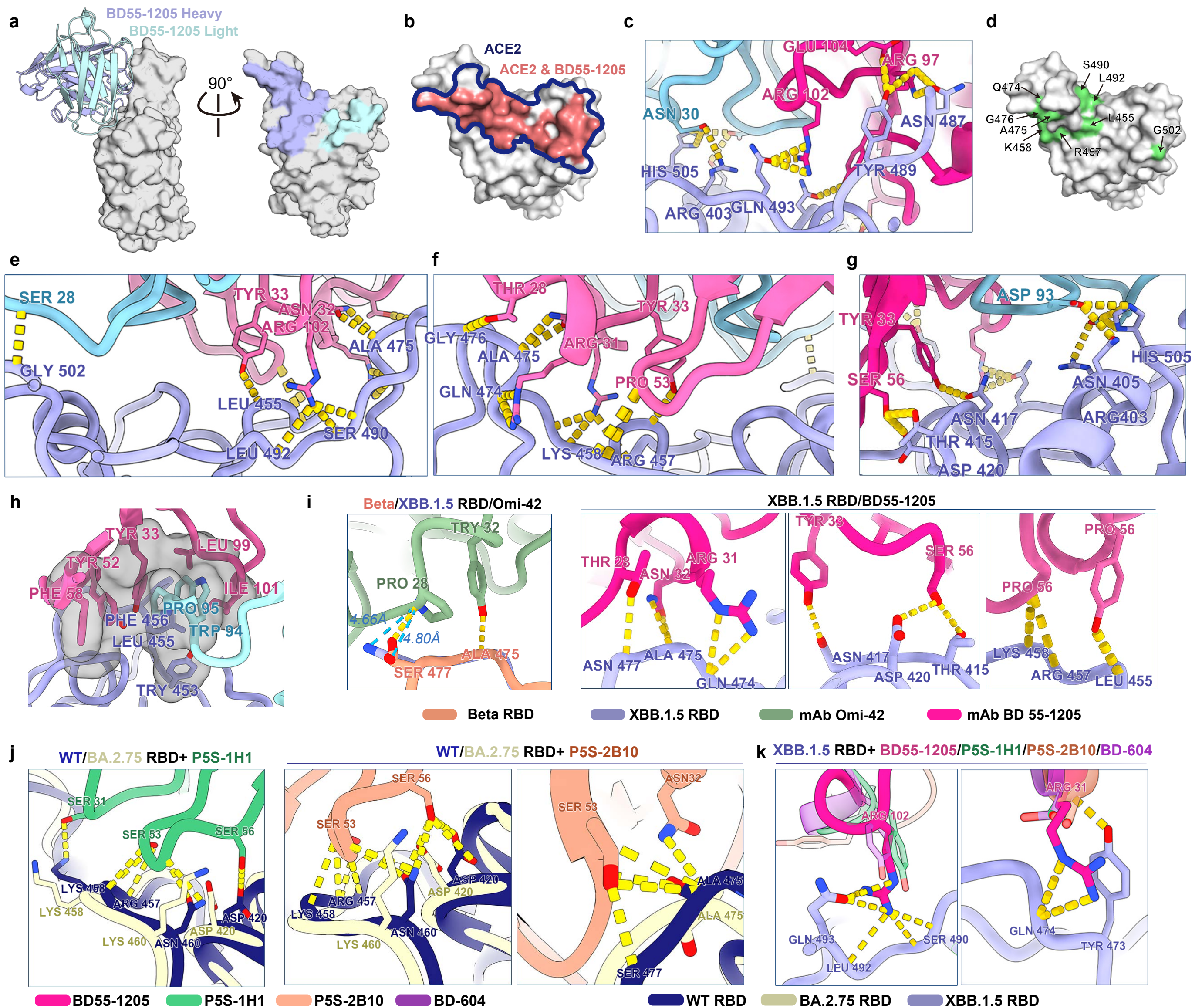

Figure 4 | Structural basis of the broad reactivity of BD55-1205

a, Structural model of SARS-CoV-2 XBB.1.5 RBD in complex of BD55-1205 from Cryo-EM data. b, Overlap of BD55-1205 and hACE2 binding footprints on XBB.1.5 RBD. c, Polar interactions between BD55-1205 and XBB.1.5 RBD side chain atoms. d, RBD residues forming interactions with BD55-1205 via backbone atoms. e-g, Polar interactions between BD55-1205 heavy chain or light chain and XBB.1.5 RBD backbone atoms on the binding interface. Yellow dashed lines indicate potential polar interactions. RBD, heavy chain, and light chain are colored in blue, magenta, and cyan, respectively. h, Hydrophobic interaction between RBD and BD55-1205. i-k, Comparison of the RBD interactions of BD55-1205 and other NAbs (PDB: Omi-42, 7ZR7; P5S-1H1, 7XS8; P5S-2B10, 7XSC; BD-604, 8HWT) targeting similar epitope (Class 1).

bioRxiv preprint doi: https://doi.org/10.1101/2024.04.16.589454; this version posted April 18, 2024. The copyright holder for this preprint (which was not certified by peer review) is the author/funder, who has granted bioRxiv a license to display the preprint in perpetuity. It is made available under aCC-BY-NC-ND 4.0 International license.

Figure 5

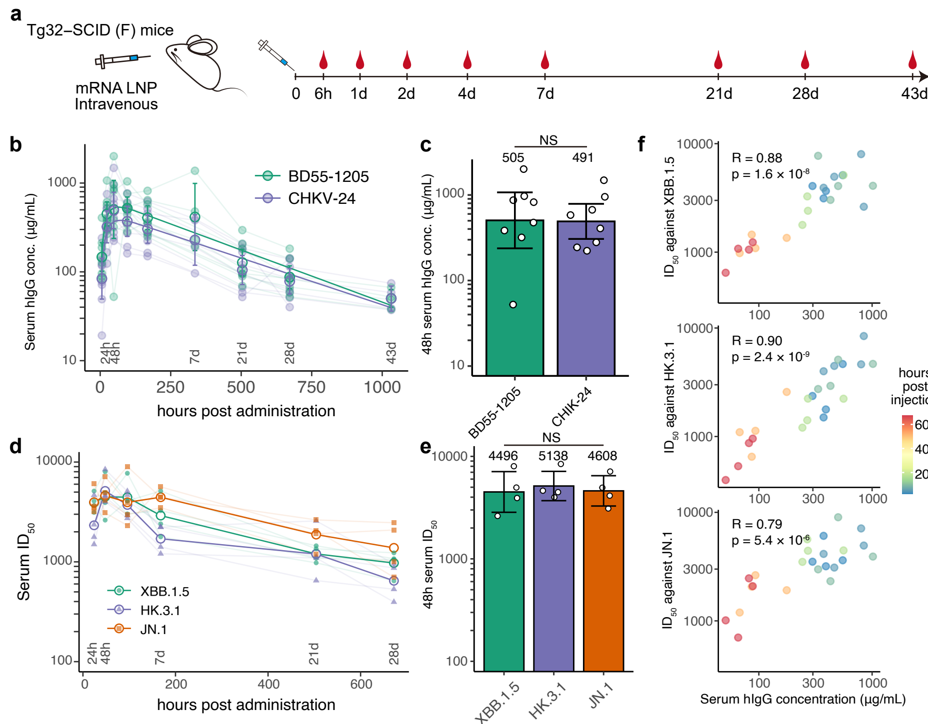

Figure 5 | mRNA delivery of BD55-1205 in mice

a, A schematic of the experimental design for deliver of BD55-1205 by mRNA-LNPs in Tg32-SCID mice. Female mice, 4 per group, received 0.5 mg/kg dose by intravenous injection on day 0 and serum was collected at indicated intervals. b, Serum concentration of BD55-1205 and a benchmark antibody CHKV-24 plotted over time. Geometric mean with error (95% confidence interval) is shown by outlined circles with error bars; solid symbols indicate individual animals. A biexponential curve was fitted to the data. Two independent in vivo experiments were combined, each with n=4 animals per group. c, Peak serum concentration, occurring at 48 hours post LNP administration, for BD55-1205 and CHKV-24. Bar height and number above the bar indicate the geometric mean; error bars indicate error (95% confidence interval); empty symbols indicate individual animals. NS, not significant (Wilcoxon rank-sum test). d, Half-maximal inhibitory dilutions (ID50) of the mice sera against XBB.1.5, HK.3.1, and JN.1 VSV pseudoviruses for BD55-1205 plotted over time. Geometric mean values are shown as the colored empty circles and lines. The ID50 of serum sample from each mouse is shown as colored points and lines. e, Peak serum ID50 at 48 hours post administration in mice that received BD55-1205 mRNA against the three indicated viral variants. Bar height and number above the bar indicate the geometric mean; error bars indicate error (95% confidence interval); empty symbols indicate individual animals. NS, not significant (Wilcoxon rank-sum test applied to any pair of variants). f, Scatter plots showing the correlation between serum hIgG concentrations and the ID50 against the three variants at indicated timepoints. Pearson correlation coefficients (R) and the corresponding significance p-values are annotated.

bioRxiv preprint doi: https://doi.org/10.1101/2024.04.16.589454; this version posted April 18, 2024. The copyright holder for this preprint (which was not certified by peer review) is the author/funder, who has granted bioRxiv a license to display the preprint in perpetuity. It is made available under aCC-BY-NC-ND 4.0 International license.

Extended Data Fig. 1

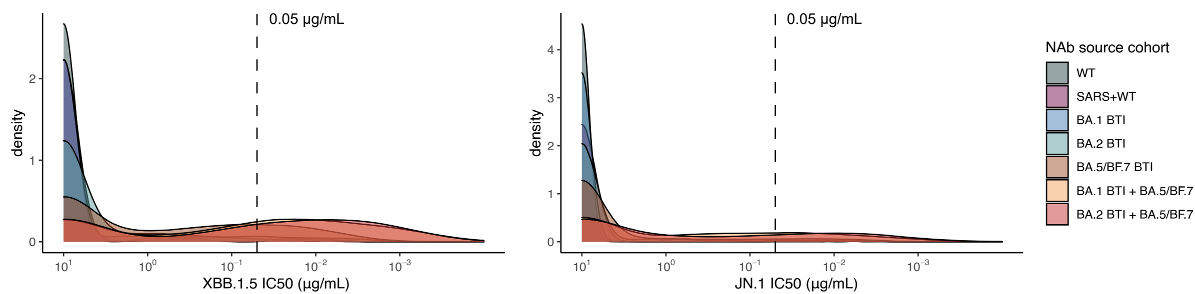

bioRxiv preprint doi: https://doi.org/10.1101/2024.04.16.589454; this version posted April 18, 2024. The copyright holder for this preprint (which was not certified by peer review) is the author/funder, who has granted bioRxiv a license to display the preprint in perpetuity. It is made available under aCC-BY-NC-ND 4.0 International license.

Extended Data Fig. 2

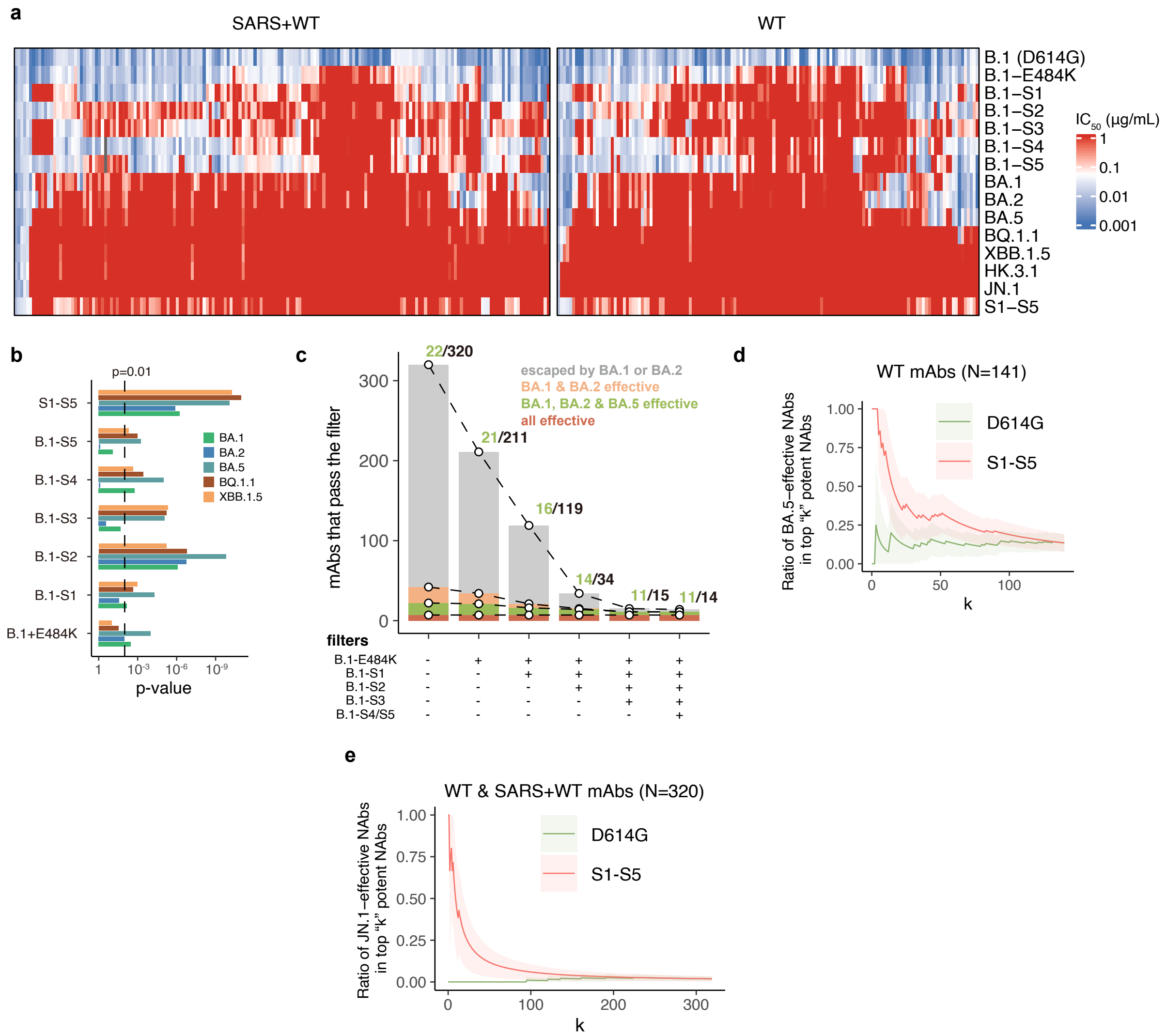

bioRxiv preprint doi: https://doi.org/10.1101/2024.04.16.589454; this version posted April 18, 2024. The copyright holder for this preprint (which was not certified by peer review) is the author/funder, who has granted bioRxiv a license to display the preprint in perpetuity. It is made available under aCC-BY-NC-ND 4.0 International license.

Extended Data Fig. 3

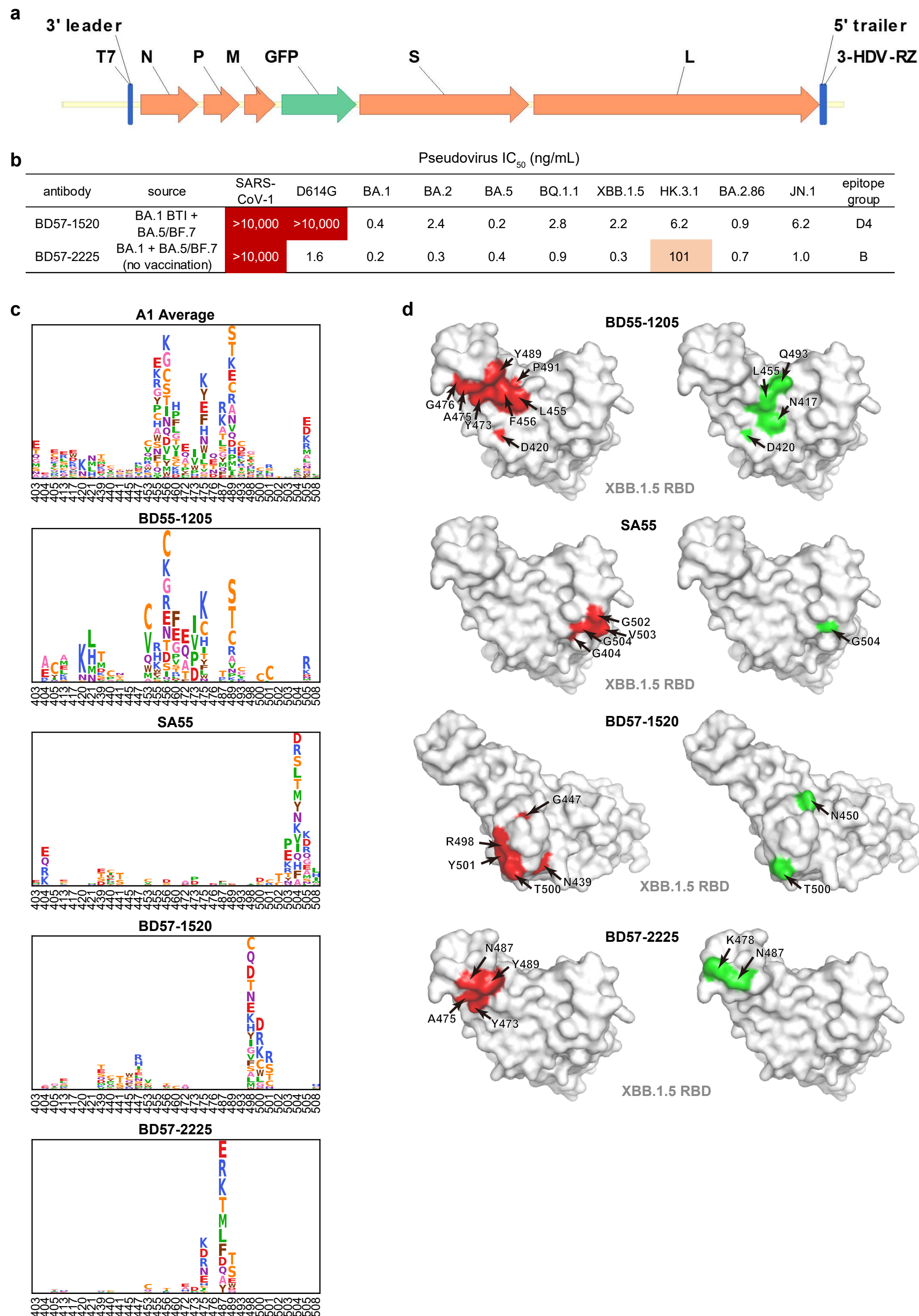

Pseudovirus IC_{50} (ng/mL)

antibody	source	SARS-CoV-1	D614G	BA.1	BA.2	BA.5	BQ.1.1	XBB.1.5	HK.3.1	BA.2.86	JN.1	epitope group
BD57-1520	BA.1 BTI + BA.5/BF.7	>10,000	>10,000	0.4	2.4	0.2	2.8	2.2	6.2	0.9	6.2	D4
BD57-2225	BA.1 + BA.5/BF.7 (no vaccination)	>10,000	1.6	0.2	0.3	0.4	0.9	0.3	101	0.7	1.0	B

bioRxiv preprint doi: https://doi.org/10.1101/2024.04.16.589454; this version posted April 18, 2024. The copyright holder for this preprint (which was not certified by peer review) is the author/funder, who has granted bioRxiv a license to display the preprint in perpetuity. It is made available under aCC-BY-NC-ND 4.0 International license.

Extended Data Fig. 4

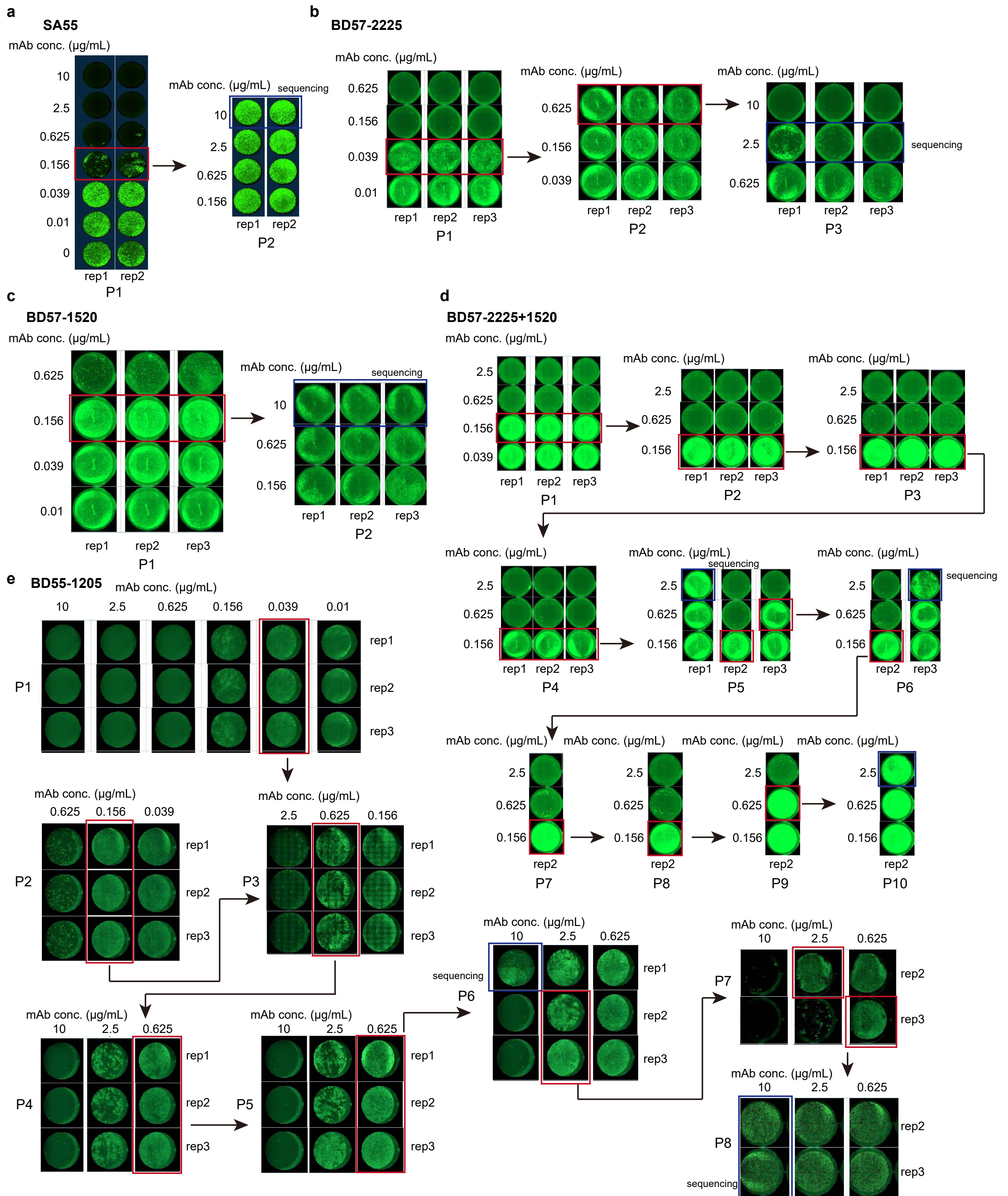

bioRxiv preprint doi: https://doi.org/10.1101/2024.04.16.589454; this version posted April 18, 2024. The copyright holder for this preprint (which was not certified by peer review) is the author/funder, who has granted bioRxiv a license to display the preprint in perpetuity. It is made available under aCC-BY-NC-ND 4.0 International license.

Extended Data Fig. 5

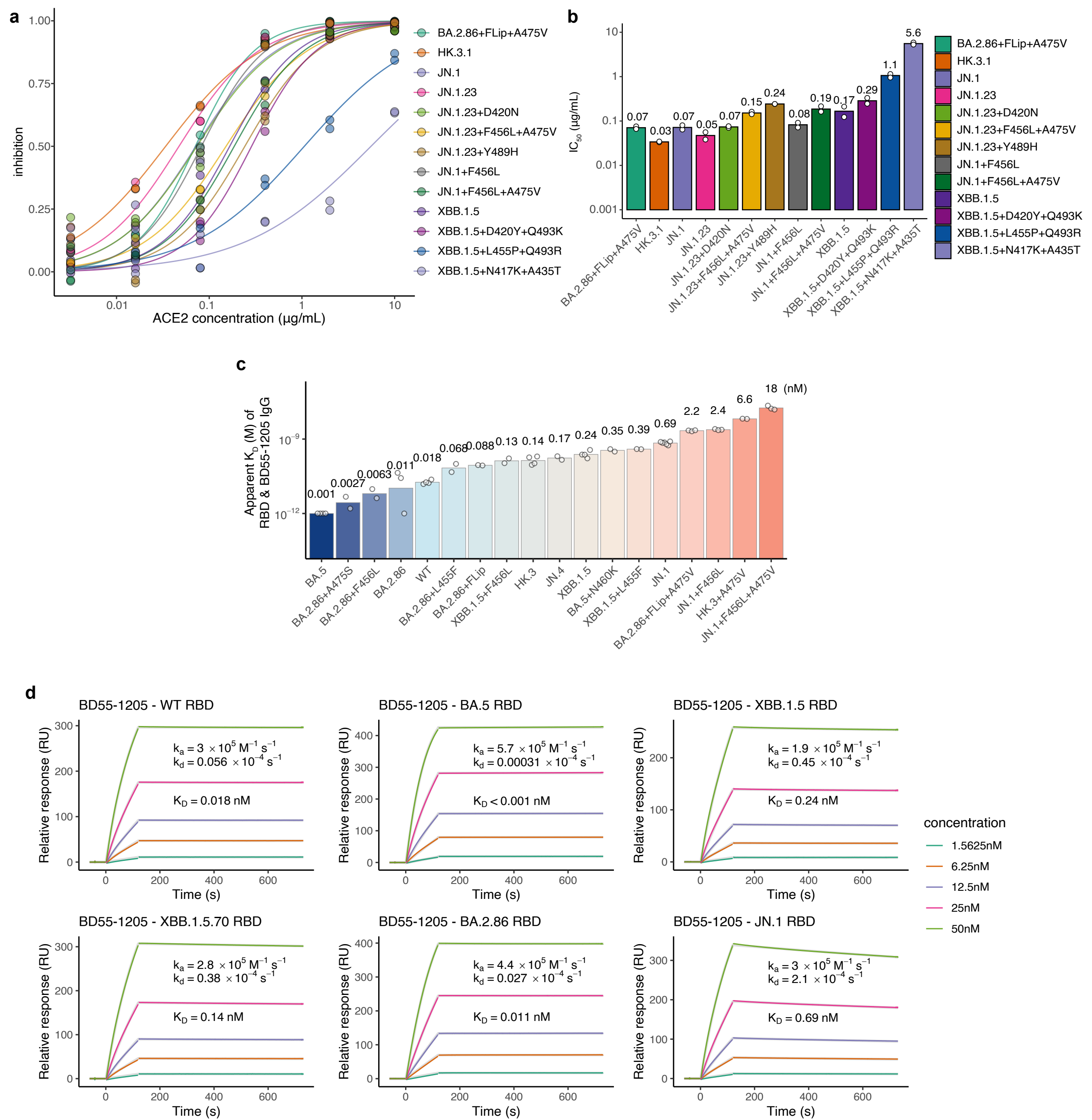

bioRxiv preprint doi: https://doi.org/10.1101/2024.04.16.589454; this version posted April 18, 2024. The copyright holder for this preprint (which was not certified by peer review) is the author/funder, who has granted bioRxiv a license to display the preprint in perpetuity. It is made available under aCC-BY-NC-ND 4.0 International license.

Extended Data Fig. 6

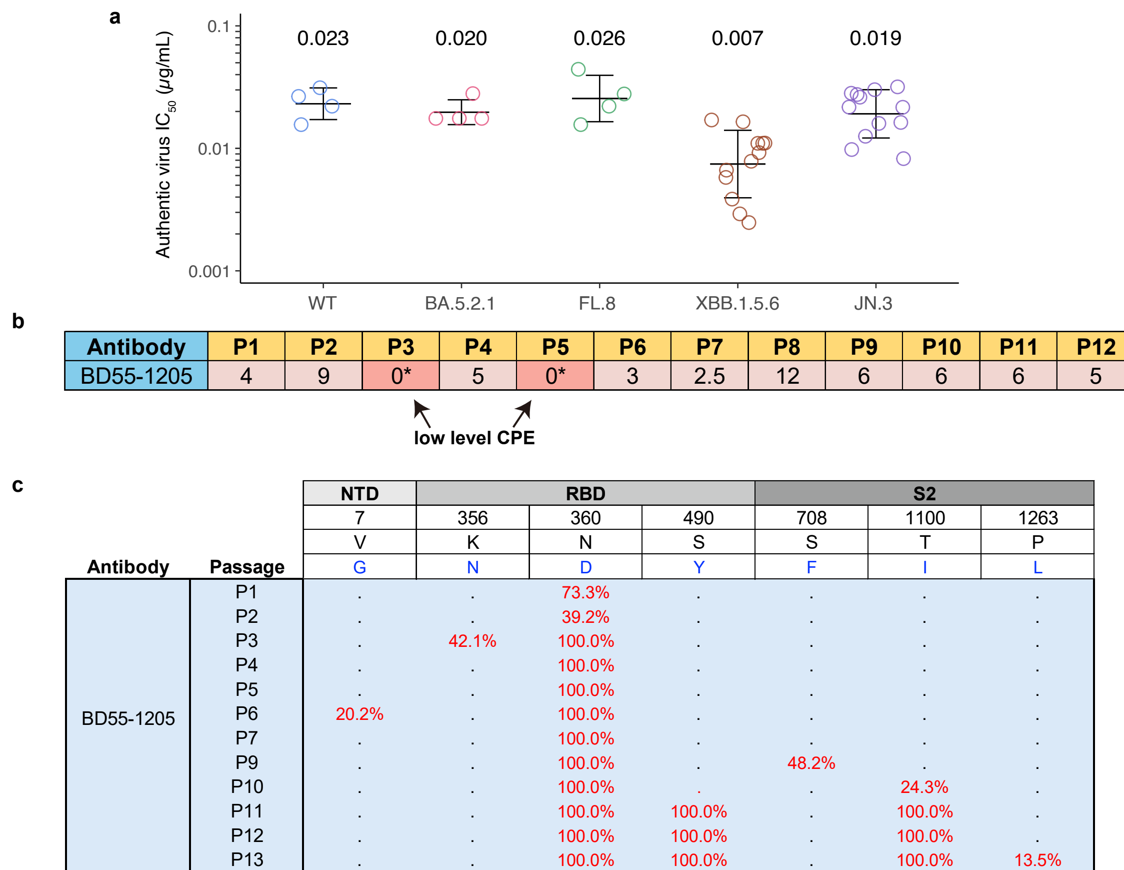

b

Antibody	P1	P2	P3	P4	P5	P6	P7	P8	P9	P10	P11	P12
BD55-1205	4	9	0*	5	0*	3	2.5	12	6	6	6	5

c

		NTD	RBD			S2		
		7	356	360	490	708	1100	1263
		V	K	N	S	S	T	P
Antibody	Passage	G	N	D	Y	F	I	L
BD55-1205	P1	.	.	73.3%	.	.	.	.
	P2	.	.	39.2%	.	.	.	.
	P3	.	42.1%	100.0%	.	.	.	.
	P4	.	.	100.0%	.	.	.	.
	P5	.	.	100.0%	.	.	.	.
	P6	20.2%	.	100.0%	.	.	.	.
	P7	.	.	100.0%	.	.	.	.
	P9	.	.	100.0%	.	48.2%	.	.
	P10	.	.	100.0%	.	.	24.3%	.
	P11	.	.	100.0%	100.0%	.	100.0%	.
	P12	.	.	100.0%	100.0%	.	100.0%	.
	P13	.	.	100.0%	100.0%	.	100.0%	13.5%

bioRxiv preprint doi: https://doi.org/10.1101/2024.04.16.589454; this version posted April 18, 2024. The copyright holder for this preprint (which was not certified by peer review) is the author/funder, who has granted bioRxiv a license to display the preprint in perpetuity. It is made available under aCC-BY-NC-ND 4.0 International license.

Extended Data Fig. 7

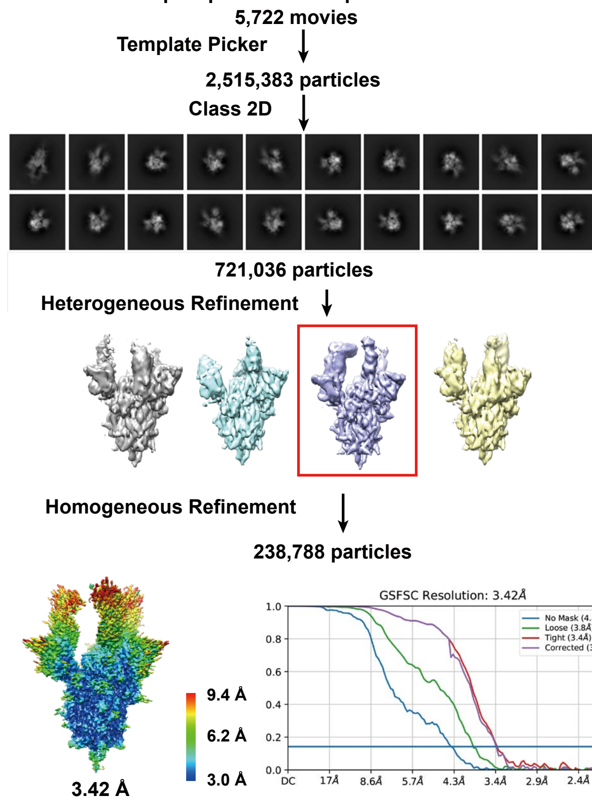

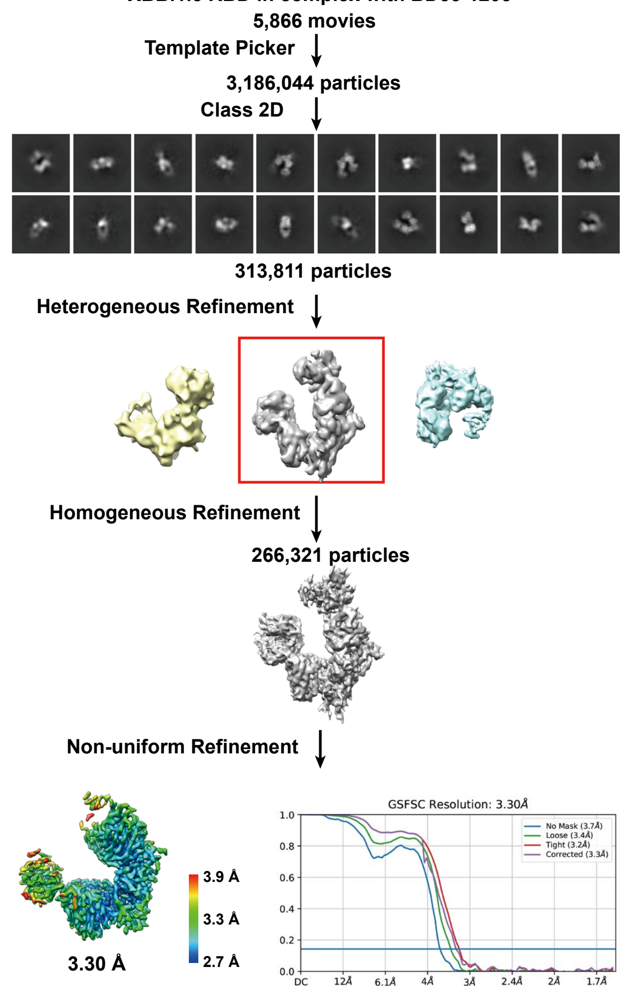

bioRxiv preprint doi: https://doi.org/10.1101/2024.04.16.589454; this version posted April 18, 2024. The copyright holder for this preprint (which was not certified by peer review) is the author/funder, who has granted bioRxiv a license to display the preprint in perpetuity. It is made available under aCC-BY-NC-ND 4.0 International license.

Extended Data Fig. 8

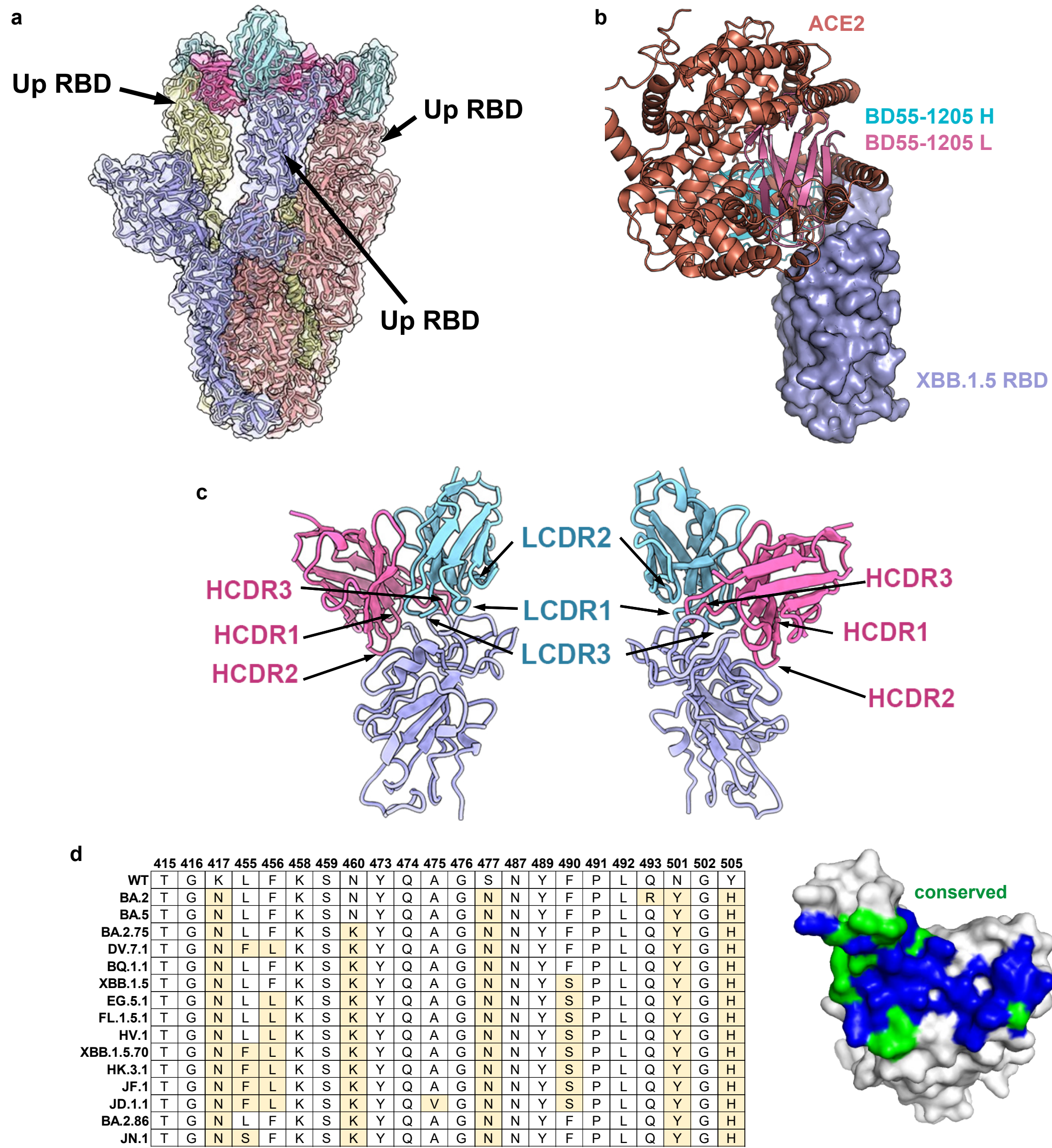

	415	416	417	455	456	458	459	460	473	474	475	476	477	487	489	490	491	492	493	501	502	505
WT	T	G	K	L	F	K	S	N	Y	Q	A	G	S	N	Y	F	P	L	Q	N	G	Y
BA.2	T	G	N	L	F	K	S	N	Y	Q	A	G	N	N	Y	F	P	L	R	Y	G	H
BA.5	T	G	N	L	F	K	S	N	Y	Q	A	G	N	N	Y	F	P	L	Q	Y	G	H
BA.2.75	T	G	N	L	F	K	S	K	Y	Q	A	G	N	N	Y	F	P	L	Q	Y	G	H
DV.7.1	T	G	N	F	L	K	S	K	Y	Q	A	G	N	N	Y	F	P	L	Q	Y	G	H
BQ.1.1	T	G	N	L	F	K	S	K	Y	Q	A	G	N	N	Y	F	P	L	Q	Y	G	H
XBB.1.5	T	G	N	L	F	K	S	K	Y	Q	A	G	N	N	Y	S	P	L	Q	Y	G	H
EG.5.1	T	G	N	L	L	K	S	K	Y	Q	A	G	N	N	Y	S	P	L	Q	Y	G	H
FL.1.5.1	T	G	N	L	L	K	S	K	Y	Q	A	G	N	N	Y	S	P	L	Q	Y	G	H
HV.1	T	G	N	L	L	K	S	K	Y	Q	A	G	N	N	Y	S	P	L	Q	Y	G	H
XBB.1.5.70	T	G	N	F	L	K	S	K	Y	Q	A	G	N	N	Y	S	P	L	Q	Y	G	H
HK.3.1	T	G	N	F	L	K	S	K	Y	Q	A	G	N	N	Y	S	P	L	Q	Y	G	H
JF.1	T	G	N	F	L	K	S	K	Y	Q	A	G	N	N	Y	S	P	L	Q	Y	G	H
JD.1.1	T	G	N	F	L	K	S	K	Y	Q	V	G	N	N	Y	S	P	L	Q	Y	G	H
BA.2.86	T	G	N	L	F	K	S	K	Y	Q	A	G	N	N	Y	F	P	L	Q	Y	G	H
JN.1	T	G	N	S	F	K	S	K	Y	Q	A	G	N	N	Y	F	P	L	Q	Y	G	H

bioRxiv preprint doi: https://doi.org/10.1101/2024.04.16.589454; this version posted April 18, 2024. The copyright holder for this preprint (which was not certified by peer review) is the author/funder, who has granted bioRxiv a license to display the preprint in perpetuity. It is made available under aCC-BY-NC-ND 4.0 International license.

Extended Data Fig. 9

a

BD55-1205

Hydrogen bonds

RBD	H Chain	RBD	L Chain
T415-OG1 ···	S56-OG	R403-NH2 ···	N30-OD1
N417-OD1 ···	Y33-OH	N405-OD1 ···	D93-OD2
D420-OD2 ···	S56-OG	N417-ND2 ···	W94-O
Y421-OH ···	P53-N	Y501-OH ···	N30-O
Y421-OH ···	G54-N	G502-N ···	S28-O
L455-O ···	Y33-OH	H505-ND1 ···	N30-ND2
R457-O ···	P53-O	H505-ND1 ···	G92-O
K458-O ···	P53-O	H505-NE2 ···	N30-ND2
Y473-OH ···	R31-O		
Q474-O ···	R31-NE		
Q474-O ···	R31-NH2		
A475-O ···	N32-OD1		
A475-O ···	N32-ND2		
G476-O ···	T28-OG1		
N487-OD1 ···	R97-NH1		
N487-OD1 ···	R97-NH2		
N487-ND2 ···	G26-O		
Y489-OH ···	R97-NH2		
Y489-OH ···	E104-OE1		
S490-N ···	R102-NH2		
S490-O ···	R102-NH2		
L492-O ···	R102-NH2		
Q493-OE1 ···	R102-NE		
Q493-OE1 ···	R102-NH1		
Q493-OE1 ···	R102-NH2		

Salt bridges

RBD	L Chain
H505-NE2 ···	D93-OD2

b

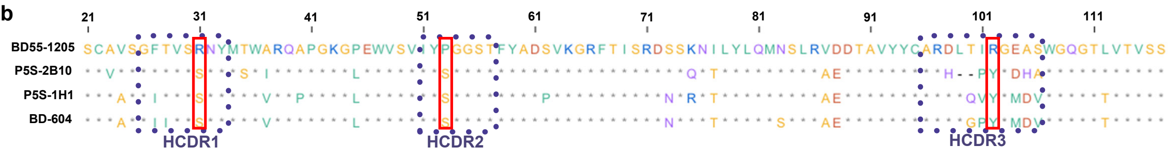

c

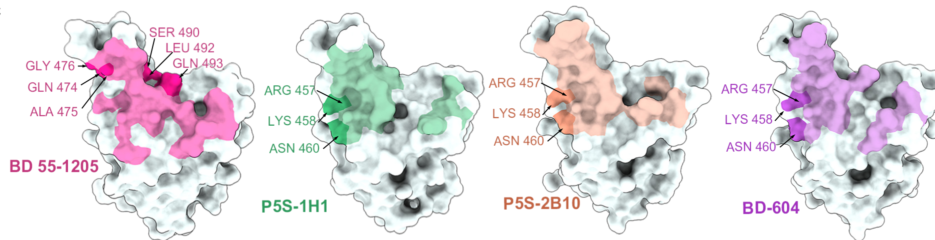

d

Pseudovirus IC_{50} (μg/mL)	BA.5	HK.3.1	JN.1	JN.1 +F456L	JN.1 +F456L +A475V
BD55-1205	0.001	0.006	0.004	0.012	0.021
BD55-1205 (H-R31S)	0.003	0.010	0.007	0.008	0.013
BD55-1205 (H-P53S)	0.003	0.016	0.009	0.008	0.019
BD55-1205 (H-R102Y)	0.002	0.002	0.003	0.009	0.013
BD55-1205-GLHV	0.002	0.005	0.004	0.010	>10

e